TRAIP promotes DNA damage response during genome replication and is mutated in primordial dwarfism

Harley, Margaret E; Murina, Olga ; Leitch, Andrea ; Higgs, Martin; Bicknell, Louise S; Yigit, Gökhan ; Blackford, Andrew N ; Zlatanou, Anastasia; Mackenzie, Karen J ; Reddy, Kaalak ; Halachev, Mihail ; McGlasson, Sarah ; Reijns, Martin A M ; Fluteau, Adeline ; Martin, Carol-Anne ; Sabbioneda, Simone ; Elcioglu, Nursel H ; Altmüller, Janine ; Thiele, Holger ; Greenhalgh, Lynn

DOI:
10.1038/ng.3451

Document Version
Peer reviewed version

Citation for published version (Harvard):
Harley, ME, Murina, O, Leitch, A, Higgs, M, Bicknell, LS, Yigit, G, Blackford, AN, Zlatanou, A, Mackenzie, KJ, Reddy, K, Halachev, M, McGlasson, S, Reijns, MAM, Fluteau, A, Martin, C-A, Sabbioneda, S, Elcioglu, NH, Altmüller, J, Thiele, H, Greenhalgh, L, Chessa, L, Maghnie, M, Salim, M, Bober, MB, Nürnberg, P, Jackson, SP, Hurles, ME, Wollnik, B, Stewart, G & Jackson, A 2016, 'TRAIP promotes DNA damage response during genome replication and is mutated in primordial dwarfism', *Nature Genetics*, vol. 48, no. 1, pp. 36-43. https://doi.org/10.1038/ng.3451

TRAIP promotes DNA damage response during genome replication and is mutated in primordial dwarfism

Margaret E. Harley[1,18], Olga Murina[1,18], Andrea Leitch[1], Martin R. Higgs[2], Louise S. Bicknell[1,17], Gökhan Yigit[3,4,5], Andrew N. Blackford[6], Anastasia Zlatanou[2], Karen J. Mackenzie[1], Kaalak Reddy[1], Mihail Halachev[1], Sarah McGlasson[1], Martin A. M. Reijns[1], Adeline Fluteau[1,], Carol-Anne Martin[1], Simone Sabbioneda[7], Nursel H. Elcioglu[8], Janine Altmüller[3,9], Holger Thiele[9], Lynn Greenhalgh[10], Luciana Chessa[11], Mohamad Maghnie[12], Mahmoud Salim[8], Michael B. Bober[13], Peter Nürnberg[4,5,9], Stephen P. Jackson[6,14,15], Matthew E. Hurles[15], Bernd Wollnik[3,4,5,16], Grant S. Stewart[2], Andrew P. Jackson[1].

Affiliations:

1. MRC Human Genetics Unit, IGMM, University of Edinburgh, Edinburgh, EH4 2XU, UK
2. Institute of Cancer and Genomic Sciences, College of Medical and Dental Sciences, University of Birmingham, Birmingham, B15 2TT, UK
3. Institute of Human Genetics, University Hospital Cologne, University of Cologne, 50931 Cologne, Germany
4. Center for Molecular Medicine Cologne (CMMC), University of Cologne, 50931 Cologne, Germany
5. Cologne Excellence Cluster on Cellular Stress Responses in Aging-Associated Diseases (CECAD), University of Cologne, 50931 Cologne, Germany
6. The Gurdon Institute, University of Cambridge, Cambridge, CB2 1QN, UK
7. Istituto di Genetica Molecolare, CNR, 27100 Pavia, Italy
8. Department of Pediatric Genetics, Marmara University Pendik Hospital, Istanbul, Turkey
9. Cologne Center for Genomics (CCG), University of Cologne, 50931 Cologne, Germany
10. Cheshire and Merseyside Clinical Genetics Service, Liverpool Women's Hospital, Liverpool, L12 2AP, UK
11. Department of Clinical and Molecular Medicine, University Sapienza, A.O.S. Andrea, I-00189 Roma, Italy
12. Department of Pediatrics, IRCCS, Giannina Gaslini, University of Genova, 16147 Genova, Italy
13. Nemours/Alfred I. duPont Hospital for Children, Wilmington, Delaware 19803, USA
14. Department of Biochemistry, University of Cambridge, Cambridge, CB2 1QN, UK

15. Wellcome Trust Sanger Institute, Cambridge, CB10 1SA, UK
16. Institute of Human Genetics, University Medical Centre Göttingen, 37073 Göttingen, Germany
17. Present address: Department of Pathology, Dunedin School of Medicine, University of Otago, Dunedin, New Zealand
18. These authors contributed equally to this work.

Correspondence to APJ, andrew.jackson@igmm.ed.ac.uk, GSS, g.s.stewart@bham.ac.uk, or BW, bwollnik@uni-koeln.de

Article abstract

DNA lesions encountered by replicative polymerases threaten genome stability and cell cycle progression. Here we report the identification of mutations in *TRAIP*, encoding an E3 RING ubiquitin ligase, in patients with microcephalic primordial dwarfism/Seckel syndrome. We establish that TRAIP relocalizes to sites of DNA damage where it is required for optimal phosphorylation of H2AX and RPA2 during S-phase in response to UV irradiation, as well as fork progression through UV-induced DNA lesions. TRAIP is necessary for efficient cell cycle progression and mutations in TRAIP therefore limit cellular proliferation, providing a potential mechanism for microcephaly and dwarfism phenotypes. Human genetics thus identifies TRAIP as a novel component of the DNA damage response to replication-blocking DNA lesions.

INTRODUCTION

The rapid cellular response to genomic insults is facilitated by signaling cascades which utilize diverse post-translational modifications, particularly ubiquitylation and phosphorylation[1,2]. Mutations in genes encoding many components of DNA damage response (DDR) signaling pathways have been identified in human disease[1], reflecting the central importance of DNA repair in maintaining cellular homeostasis. Mutations in DDR genes have been associated with increased cancer predisposition, immunodeficiency, premature ageing and neurodegeneration[3,4]. Growth restriction and microcephaly are also features of certain DNA repair disorders[5-9]. Microcephalic primordial dwarfism (MPD) represents a group of single gene disorders[10] typically inherited as autosomal recessive traits, that includes Seckel syndrome[11,12], Microcephalic Osteodysplastic Primordial Dwarfism (MOPD) syndromes[13,14] and Meier-Gorlin syndrome[15,16]. In MPD, growth is restricted prenatally and remains severely restricted postnatally, resulting in an adult height as short as 1 meter[17]. Marked reduction in brain size, manifesting as microcephaly, distinguishes MPD from other forms of dwarfism, and mutations in genes encoding components of key cellular processes, including centrosome biogenesis, mitotic spindle function, replication licensing and DNA damage repair, have been identified in these disorders[10]. Particularly, multiple components of ATR-dependent DDR signaling have been implicated in Seckel syndrome and MOPD II, including mutations in *ATR*, *ATRIP*, *RBBP8* (encoding CtIP) and *PCNT*[7,8,18,19].

To identify further primordial dwarfism genes relevant to cell cycle and DNA repair processes, we performed whole-exome sequencing (WES) on a group of primordial dwarfism patients. Here, we report the identification of *TRAIP* as a novel human disease-associated gene, and implicate the protein it encodes in regulating the DNA damage response to genotoxic lesions during replication.

RESULTS

TRAIP is a novel gene mutated in primordial dwarfism

We performed WES to establish a molecular diagnosis for a child with severe microcephalic primordial dwarfism. After filtering to remove common variants (minor allele frequency (MAF) > 0.005), analysis under a recessive inheritance model identified a homozygous nonsense mutation in *TRAIP*, c.553C>T, resulting in a premature stop codon, p.Arg185* (**Fig. 1a**). Sanger sequencing confirmed the presence of this mutation and its appropriate segregation in the family, with both parents being heterozygous carriers. The variant was not detected on sequencing of 380 control chromosomes, nor was it present in 1000 Genomes, EVS or EXaC public variant databases, in keeping

with it being a rare recessive pathogenic mutation. Sanger resequencing of the coding exons and splice junctions of *TRAIP* in 262 primary microcephaly and primordial dwarfism patients identified a second patient, homozygous for the same mutation, p.Arg185*. Notably the two patients were born to non-consanguineous parents and originated from different countries with the families having no known relationship. However, high density genome-wide SNP genotyping demonstrated regions of homozygosity surrounding TRAIP in both patients of 4.6 and 8.4Mb respectively, consistent with unrecognized parental relatedness in each family (**Supplementary Fig. 1a**). As well, analysis of genome-wide SNP genotype data using FEstim[20] provided an inbreeding coefficient estimate of 0.003 for P2, equivalent to the inbreeding coefficient of 3rd cousin parents and also consistent with unknown parental consanguinity in this family (**Supplementary Fig. 1b**). Furthermore a 4.3 Mb homozygous haplotype was shared between P1 and P2 for the region immediately surrounding TRAIP, signifying a distant familial link with shared ancestry many generations previously despite their geographical separation (**Supplementary Fig. 1a**).

Additional WES on a cohort of patients with a presumptive diagnosis of Seckel syndrome (n=28), identified a further consanguineous family with a different mutation in *TRAIP.* In this family, a homozygous missense mutation was identified, c.52C>T, resulting in an arginine to cysteine substitution at codon 18 (p.Arg18Cys) (**Fig. 1a**). This highly conserved residue (**Fig. 1b**) lies within a RING domain, with the mutation resulting in a large physiochemical change, predicted bioinformatically to be deleterious (Alamut, Interactive Biosoftware Inc). The addition of a further cysteine residue is thought likely to be structurally deleterious, given that RING domains are defined by a specific motif of cysteine and histidine residues that bind zinc divalent cations to establish their tertiary structure[21].

The clinical phenotype of all three patients was remarkably similar (**Fig. 1**, **Table 1**, **Supplementary Note**). They shared almost identical growth parameters, with global growth failure of prenatal onset and extreme disproportionate microcephaly (**Fig. 1c**, **Table 1**). Neuroimaging demonstrated reduced cerebral cortical size with simplified gyral folding (**Fig. 1d**). Craniofacial similarities included a narrow elongated face and micrognathia (**Fig. 1e**). Additionally, significant morbidity from infections was evident. Patient 1 (P1) and Patient 2 (P2) had frequent lower respiratory tract infections, with P1 dying of respiratory failure aged 10 years as a result of chronic lung disease. Furthermore, P1 had two siblings who died in early infancy[22]. However, aside from P2 who had a persistent lymphopenia, there was no evidence of adaptive immune deficits on clinical investigation.

On the basis of the mutations identified and phenotypic similarities between patients, we concluded that *TRAIP* was a novel gene associated with primordial dwarfism. TRAIP (TNF receptor associated

factor (TRAF)-interacting partner; TRIP; RNF206) is a RING domain-type E3 ubiquitin ligase[23] originally identified as a negative regulator of innate immune signaling[24]. As it ubiquitylates TBK1[25], a key transducer of Toll-receptors and RIG-I, this could explain the recurrent respiratory illnesses in the patients; however the mechanistic basis for the primordial dwarfism phenotype was less evident. Therefore we proceeded to investigate the functional basis for the growth-related phenotypes.

TRAIP protein levels are markedly depleted in patient cells

We obtained cell lines from all three patients and characterized these to confirm the deleterious effect of mutations on the TRAIP protein. The Arg185* mutation introduces a premature stop codon in exon 7 and would be expected to cause nonsense-mediated decay of the *TRAIP* transcript. RT-PCR was therefore performed on RNA extracted from patient cells to assess transcript levels. This demonstrated marked reduction in *TRAIP* mRNA both in the immortalized lymphoblastoid cell line from P1 and a primary fibroblast cell line from P2 (**Fig. 2a**). Notably, low levels of residual full-length mRNA as well as alternatively spliced transcripts were evident. Cloning and sequencing of these RT-PCR products demonstrated that the latter included transcripts that are predicted to produce in-frame deletions of the TRAIP protein of 37 or 99 amino acids (**Fig. 2a**).

Immunoblotting was next performed to establish the consequence of the mutation at the protein level. TRAIP protein levels were greatly reduced in both patient cell lines P1 and P2 carrying the Arg185* mutation (**Fig. 2b**). A TRAIP protein of comparable size (47 kDa) to wild-type TRAIP (53 kDa) was only detectable on prolonged immunoblot exposure (**Supplementary Fig. 2**) while a truncated protein isoform of 184 amino acids was not observed, despite the polyclonal antibody (raised against residues 1-270) being able to efficiently detect both *in vitro* synthesized truncated and full-length proteins (**Supplementary Fig. 3**). In conjunction with RT-PCR findings, detection of residual TRAIP protein expression suggests that the mutation is a severe hypomorph, likely compromising, but not completely abrogating TRAIP cellular function. Consistent with this, a knockout mouse model established that *Traip* is essential for early embryonic development, with embryonic lethality seen at gastrulation and a reduction in cell number and embryo growth occurring as early as E5.5[26].

The Arg18Cys mutation had no effect on transcript levels (**Supplementary Fig. 4**), but also resulted in marked reduction of TRAIP protein levels in primary fibroblasts derived from patient P3 (**Fig. 2b**), probably reflecting reduced protein stability resulting from the missense mutation. We therefore

concluded that patient TRAIP mutations would likely lead to substantial impairment of its cellular E3 ligase activity through depletion of overall protein levels.

TRAIP localizes to sites of UV-induced DNA damage

Phenotypically, TRAIP patients were reminiscent of individuals with Seckel syndrome that have defects in ATR pathway signaling[7,8], particularly with their disproportionately reduced head size. We therefore postulated that TRAIP could be a DDR protein acting in this pathway. Consistent with this, live-imaging of GFP-TRAIP protein demonstrated rapid re-localization from a pan-nuclear distribution to sites of DNA damage after UV laser microirradiation, irrespective of addition of BrdU as a DNA damage sensitizer (**Fig. 3a**). Colocalization was observed both with γH2AX and RFP-PCNA (**Fig. 3b**). Proximity ligation assays (PLA) detected GFP-TRAIP in close proximity (<40 nm) to PCNA in undamaged cells, suggesting it can be present at replication foci in undamaged cells. This association was substantially enriched after UV-C irradiation (**Fig. 3c**, **d**, $p < 0.001$), consistent with TRAIP localizing with PCNA at sites of DNA damage. Relocalisation of TRAIP to sites of UV-induced DNA damage was confirmed using localized UV-C irradiation through 3 μm isopore membrane filters, after which GFP-TRAIP was detected in irradiated regions, along with multiple DNA damage repair markers, including γH2AX and RPA2 (**Fig. 3e**). Notably, TRAIP was a highly significant hit in a recently reported high-throughput mass spectroscopy screen for proteins recruited to replication blocking DNA lesions[27]. As well as re-localizing to DNA damage sites, we also noted that TRAIP protein levels were regulated by DNA damage, with proteasome-mediated degradation observed at later time points after UV treatment (**Supplementary Fig. 5**), similar to certain DDR proteins involved in repair of UV lesions[28].

TRAIP is required for RPA2 and H2AX phosphorylation in S-phase

To assess whether TRAIP was a novel component of ATR-dependent DDR signaling, siRNA-depleted HeLa cells were irradiated with 10 J/m^2 UV and a time course was performed to monitor activation of this signaling pathway. Unlike ATR/ATRIP deficient cells[7,8], ATR-mediated phosphorylation of the downstream kinase CHK1 was not impaired by TRAIP depletion (**Fig. 4a**). Additionally, phosphorylation of the ATR substrates NBS1, SMC1 and Ser33-RPA2, as well as the activation of ATM and DNA-PK were also unaffected by TRAIP knockdown (**Fig. 4a**, **Supplementary Fig. 6a**, **b**). However, a striking reduction in phosphorylation of Ser4/Ser8-RPA2 and H2AX was seen in HeLa cells

after TRAIP siRNA and in patient fibroblasts (**Fig. 4b**-**e**). Complementation of TERT-immortalized P2 fibroblasts ($P2^{TERT}$) by retroviral transduction of wild-type TRAIP ($P2^{TERT+TRAIP}$) restored RPA2/H2AX phosphorylation to normal levels after UV-C irradiation in $P2^{TERT+TRAIP}$ cells, confirming that these phosphorylation defects were directly due to loss of TRAIP (**Fig. 4f**, **Supplementary Fig. 6c**). Overall, phosphorylation of other ATR, ATM and DNA-PK substrates was comparable between $P2^{TERT}$ and $P2^{TERT+TRAIP}$ cells (**Supplementary Fig. 6d**). Given this and the normal level of DNA damage-induced phosphorylation of multiple downstream substrates of ATR in siTRAIP-depleted cells, along with a normal G2/M checkpoint in response to UV irradiation (**Supplementary Fig. 6e**), we concluded that TRAIP deficiency did not give rise to a general defect in ATR signaling, but rather compromised phosphorylation of RPA and H2AX following the induction of UV damage.

Since DNA damage response to UV lesions occurs throughout the cell cycle, we next investigated when TRAIP is required to promote RPA2 and H2AX phosphorylation. Using quantitative immunofluorescence, we found that Ser4/Ser8-RPA2 and H2AX phosphorylation induced by UV-C exposure was significantly reduced in EdU-labeled TRAIP patient $P2^{TERT}$ cells but not in EdU-negative cells, indicating that TRAIP is specifically required during S-phase for optimal DNA damage-dependent phosphorylation of these proteins (**Fig. 4g**, **Supplementary Fig. 7**). Given that pSer4/Ser8-RPA2 has been associated with the resection of DNA double strand breaks (DSBs), a process that may occur when replication forks encounter UV lesions during S-phase, we considered whether differences in DSBs in patient cells could account for the altered RPA2/H2AX phosphorylation. To assess this, we performed neutral comet assays, which demonstrated equal levels of DSBs in TRAIP patient and control primary fibroblast cell lines after UV-irradiation (**Supplementary Fig. 8**). This indicated that reduced RPA2/H2AX phosphorylation was not a consequence of altered frequency of DSB formation. We therefore concluded that TRAIP is required for optimal H2AX and RPA2 phosphorylation in response to UV-induced damage encountered in S-phase.

Loss of TRAIP impairs cellular proliferation

We next considered how *TRAIP* mutations might reduce organism growth. Many primordial dwarfism genes are thought to cause reduced size through lowering the efficiency of cellular proliferation[10]. As TRAIP is required for efficient cell proliferation both in human primary cells and during mammalian development[26,29], we assessed the consequences of these mutations on growth rates of primary patient cell lines. We found that doubling times of patient fibroblasts (P2 and P3) were significantly slower than passage-matched control fibroblasts (**Fig. 5a**, **c**). Furthermore, this

growth defect was complemented by retroviral transduction of patient cells with wild-type TRAIP (**Fig. 5b**), demonstrating that impaired proliferation was a direct consequence of TRAIP loss in patient cells, and indicating that prolonged cell cycle likely underlies the patient dwarfism phenotype.

To further characterize these cell cycle effects, we performed BrdU-pulse chase flow cytometry time courses using isogenic systems. Both TRAIP-depleted HeLa cells (**Fig. 5d**) and $P2^{TERT}$ patient cells (**Supplementary Fig. 9b**, **c**) retained higher 4n DNA content at later time points than matched controls ($p = 0.0012$, $p=0.0135$, respectively). This could not be accounted for by an increased percentage of mitotic cells (**Supplementary Fig. 9a**), and therefore represented an increase in late S-phase and/or G2 cells consistent with a replicative origin for the cell cycle delay.

To gain a further understanding of TRAIP's role during replication, we then examined replication fork dynamics in patient cells by DNA fiber analysis in patient cells. Replication fork velocity, inter-origin distance and fork stalling (1^{st} label termination events) were not significantly altered in untreated TRAIP patient cells (**Supplementary Fig. 10**), suggesting that TRAIP deficiency does not result in significant global DNA replication defects. Given that TRAIP is required for efficient progression through S-phase and S-phase-specific alterations in RPA2/H2AX phosphorylation after DNA damage induction, we postulated that TRAIP is instead required when the replication fork encounters genotoxic lesions. Consistent with this, following UV irradiation TRAIP patient cells exhibited significantly increased levels of fork stalling (**Fig. 6a**), and consequently substantially reduced levels of ongoing replicating forks. Moreover, while overall fork velocities were slowed in TRAIP patient cells after UV-C irradiation at rates comparable to control cells (**Supplementary Fig. 11a**), substantial fork asymmetry in TRAIP-deficient cells was observed (**Fig. 6b, c**), indicative of a problem with fork progression past bulky UV adducts. Importantly, $P2^{TERT+TRAIP}$ complemented cells exhibited normal levels of fork stalling (**Supplementary Fig. 11b**) and fork symmetry following UV-C irradiation (**Supplementary Fig. 11c**), establishing that TRAIP was specifically required to prevent fork stalling at UV lesions. Notably, levels of new origin firing were not increased in UV-C treated patient fibroblasts (**Fig. 6a**), indicating that the ATR-dependent intra-S-phase checkpoint remained intact. In contrast to UV, replication stress induced by low dose aphidicolin, or treatment with a cross-link inducing agent, mitomycin C (MMC), did not result in increased fork asymmetry in TRAIP patient cells compared with control cells (**Supplementary Fig. 11c**-**e**). Likewise, MMC treatment did not cause increased fork stalling in TRAIP-deficient cells (**Supplementary Fig. 11c**, **d**). Normal levels of fork recovery were also seen following replication fork stalling after hydroxyurea (HU) treatment (**Supplementary Fig. 12**), establishing that fork stability and replication restart are not generally impaired in TRAIP-deficient

cells. Therefore, rather than a general requirement to promote genome replication under conditions of replication stress, TRAIP appears to have a role ensuring fork progression past bulky polymerase-stalling DNA lesions such as UV-photo-products.

DISCUSSION

Here, we report the identification of *TRAIP* as a human disease-associated gene and implicate it in DNA damage response to genotoxic lesions during genome replication. DNA damage encountered during S-phase is especially problematic, with substantial risks of mutation and/or genomic rearrangements arising from replication intermediates. Hence, multiple cellular mechanisms are employed to ensure replication fork stability and appropriate repair of DNA lesions[30]. Given our data demonstrating increased fork stalling and asymmetry following exposure to UV, but not HU, aphidicolin or MMC, TRAIP is likely to promote repair or bypass of replication blocking lesions induced by UV, rather than playing a general role in stabilizing or promoting restart of stalled replication forks.

A role for TRAIP in promoting translesion synthesis (TLS) has been raised by a developmental study of the Drosophila ortholog *nopo* which reported polyubiquitylation of DNA polymerase η (Pol η) [31]. However, the functional relevance of this observation is unclear since experiments were carried out in the absence of UV-induced damage. As well, Pol η undergoes active deubiquitylation in mammalian cells after UV irradiation to promote its recruitment to repair sites[32]. The patient phenotype is also inconsistent with a role for TRAIP in TLS, as it is distinct from Xeroderma-Pigmentosum-variant (XP-V)[33] that results from Pol η mutations[34,35]. XP-V manifests as freckling, increased sun sensitivity and skin cancer, rather than prenatal onset growth failure and microcephaly. TRAIP patients lack such dermatological features and cancer predisposition has not been observed, although all are still children. Furthermore, TRAIP cells do not exhibit the increased ATR pathway activation seen in XP-V cells[36]. Hence, TRAIP more likely acts in a parallel, TLS-independent process, to overcome UV-C replication blocking lesions. TRAIP could instead be involved in a homologous recombination dependent mechanism to resolve such replication blocks, particularly given the role of RPA hyperphosphorylation in recruiting Rad51 after replication fork arrest[37]. Decreased RPA2 (and H2AX) phosphorylation might directly account for impaired fork progression at such UV-induced lesions, although how TRAIP promotes H2AX and RPA phosphorylation remains to be defined. TRAIP could act either by positively regulating a DDR protein

kinase at UV-induced damage sites, or suppressing PP2A or PP4 protein phosphatases that dephosphorylate γH2AX and pSer4/Ser8-RPA2[38-41].

Ubiquitylation regulates many key DNA damage response processes[2], with several DDR-associated E3 ubiquitin ligases, including BRCA1[42,43], RNF168[44] and FANCL[45] implicated in human disease. The identification of additional TRAIP ubiquitylation substrates will be important to understand the disease process, and will likely provide further insights into its role at replication blocking lesions. It also remains to be formally established if its DNA repair/replication roles are dependent on a functional RING domain, as TRAIP could have E3 ligase-independent functions.

Total cell number is the predominant determinant of size in mammals[46]. Similarly, reduced cellularity from early development is believed to cause primordial dwarfism[10], with decrease in neuronal number generated during neurogenesis underlying the microcephaly. The DNA replication machinery is implicated in other forms of microcephalic dwarfism[47-49] and replication stress during embryonic development underlies Seckel syndrome due to *ATR* mutations[50]. Therefore, perturbed cell cycle progression as a consequence of replication blocking lesions could account for the microcephaly and dwarfism present in our TRAIP patients. For the cellular studies described here, UV-C irradiation was used to generate replication-blocking lesions. Most commonly these will be bulky cyclobutane pyrimidine dimers, which are unlikely to be encountered in the embryo. However during development, different replication blocking DNA lesions are present, with potential candidates being those arising from oxidative damage[51] or aldehydes[52]. Therefore endogenous DNA lesions may pose difficulties for TRAIP-deficient cells during development, and result in depleted overall cell numbers (**Model**, **Supplementary Fig. 13**) that underlies other microcephalic dwarfism disorders [48,50,53].

In summary, we identify *TRAIP* as a novel disease-associated gene, and through investigating the cellular basis of the human phenotype establish its involvement in DDR. TRAIP promotes H2AX and RPA2 phosphorylation following replication-associated DNA damage, and assists fork progression at UV-induced replication blocking lesions. Developmentally viable alleles identified through human genetics will facilitate future studies investigating its roles during embryogenesis, while identification of TRAIP substrates and mechanistic studies of its role in response to DNA lesions encountered during DNA synthesis, will provide further insight into the key cellular processes maintaining genome stability during replication.

ACCESSION CODES and URLs

Exome sequence data has been deposited at the European Genome-phenome Archive (EGA), which is hosted by the EBI (https://www.ebi.ac.uk/ega/), under accession number EGAS00001001501.

ACKNOWLEDGMENTS

We thank the families and clinicians for their involvement and participation; N. Hastie, W. Bickmore, D. Fitzpatrick, J.-C. Acosta, M. Nowotny, V.Vitart and A. Lehmann for helpful discussions; R. Geahlen (Purdue University, USA), S. Taylor (University of Manchester), D.-J. Kleinjan (University of Edinburgh), A. Lichawska and J. Mansfeld (Gurdon Institute) for their kind gifts of reagents; J. Ding, P. Hari and E. Milz for technical assistance; E. Freyer for assistance with FACS analysis; the IGMM core sequencing service; A. Wheeler and the IGMM imaging facility for assistance with microscopy, E.Maher and A.Pearce for performing SNP genotyping arrays. This work was supported by funding from the Medical Research Council and the European Research Council (ERC, 281847) (A.P.J.), the Lister Institute for Preventative Medicine (A.P.J. and G.S.S.), Medical Research Scotland (L.S.B.), German Federal Ministry of Education and Research (BMBF, 01GM1404) and E-RARE network EuroMicro (B.W), Wellcome Trust (M. Hurles), CMMC (P.N.), Cancer Research UK (C17183/A13030) (G.S.S. and M.R.H), Swiss National Science Foundation (P2ZHP3_158709) (O.M.), AIRC (12710) and ERC/EU FP7 (CIG_303806) (S.S.), Cancer Research UK (C6/A11224) and ERC/EU FP7 (HEALTH-F2-2010-259893) (A.N.B. and S.P.J.).

AUTHOR CONTRIBUTIONS

M.E. Hurles, L.S.B., M. Halachev, G.Y., J.A., H.T., P.N., and B.W. performed exome sequencing and analysis. L.S.B., M.E. Harley, G.Y., S.M., and B.W. performed sequencing, genotyping, linkage analysis and other molecular genetics experiments. M.E. Harley, O.M., A.L., M.R.H., A.N.B., A.Z., K.R., M.A.M.R., A.F., C.-A.M., S.S., S.P.J. and G.S.S. designed and performed the cell biology experiments. N.H.E., L.G., L.C., M.M., M.S., M.B.B., K.J.M., and B.W. ascertained subjects, obtained samples and/or assisted with clinical studies. M.E. Harley and A.P.J. wrote the manuscript. The study was planned and supervised by B.W., G.S.S. and A.P.J.

COMPETING FINANCIAL INTERESTS

M.E. Hurles is a co-founder, share-holder and consultant to Congenica Ltd, a clinical diagnostics company.

REFERENCES

1. Ciccia, A. & Elledge, S.J. The DNA damage response: making it safe to play with knives. *Mol Cell* **40**, 179-204 (2010).

2. Jackson, S.P. & Durocher, D. Regulation of DNA damage responses by ubiquitin and SUMO. *Mol Cell* **49**, 795-807 (2013).

3. Slatter, M.A. & Gennery, A.R. Primary immunodeficiencies associated with DNA-repair disorders. *Expert Rev Mol Med* **12**, e9 (2010).

4. Woods, C.G. DNA repair disorders. *Arch Dis Child* **78**, 178-184 (1998).

5. German, J. Bloom's syndrome. I. Genetical and clinical observations in the first twenty-seven patients. *Am J Hum Genet* **21**, 196-227 (1969).

6. Murray, J.E. *et al.* Extreme growth failure is a common presentation of ligase IV deficiency. *Hum Mutat* **35**, 76-85 (2014).

7. O'Driscoll, M., Ruiz-Perez, V.L., Woods, C.G., Jeggo, P.A. & Goodship, J.A. A splicing mutation affecting expression of ataxia-telangiectasia and Rad3-related protein (ATR) results in Seckel syndrome. *Nat Genet* **33**, 497-501 (2003).

8. Ogi, T. *et al.* Identification of the first ATRIP-deficient patient and novel mutations in ATR define a clinical spectrum for ATR-ATRIP Seckel Syndrome. *PLoS Genet* **8**, e1002945 (2012).

9. Jackson, S.P. & Bartek, J. The DNA-damage response in human biology and disease. *Nature* **461**, 1071-1078 (2009).

10. Klingseisen, A. & Jackson, A.P. Mechanisms and pathways of growth failure in primordial dwarfism. *Genes Dev* **25**, 2011-2024 (2011).

11. Majewski, F. & Goecke, T. Studies of microcephalic primordial dwarfism I: approach to a delineation of the Seckel syndrome. *Am J Med Genet* **12**, 7-21 (1982).

12. Seckel, H.P.G. *Bird-Headed Dwarfs*, (S.Karger, Basel, 1960).

13. Majewski, F., Ranke, M. & Schinzel, A. Studies of microcephalic primordial dwarfism II: the osteodysplastic type II of primordial dwarfism. *Am J Med Genet* **12**, 23-35 (1982).

14. Majewski, F., Stoeckenius, M. & Kemperdick, H. Studies of microcephalic primordial dwarfism III: an intrauterine dwarf with platyspondyly and anomalies of pelvis and clavicles--osteodysplastic primordial dwarfism type III. *Am J Med Genet* **12**, 37-42 (1982).

15. Bongers, E.M. *et al.* Meier-Gorlin syndrome: report of eight additional cases and review. *Am J Med Genet* **102**, 115-124 (2001).

16. Gorlin, R.J., Cervenka, J., Moller, K., Horrobin, M. & Witkop, C.J., Jr. Malformation syndromes. A selected miscellany. *Birth Defects Orig Artic Ser* **11**, 39-50 (1975).

17. Rauch, A. *et al.* Mutations in the Pericentrin (PCNT) Gene Cause Primordial Dwarfism. *Science* **319,** 816-819 (2008).

18. Griffith, E. *et al.* Mutations in pericentrin cause Seckel syndrome with defective ATR-dependent DNA damage signaling. *Nat Genet* **40**, 232-236 (2008).

19. Qvist, P. *et al.* CtIP Mutations Cause Seckel and Jawad Syndromes. *PLoS Genet* **7**, e1002310 (2011).

20. Leutenegger, A.L. *et al.* Using genomic inbreeding coefficient estimates for homozygosity mapping of rare recessive traits: application to Taybi-Linder syndrome. *Am J Hum Genet* **79**, 62-66 (2006).

21. Borden, K.L. & Freemont, P.S. The RING finger domain: a recent example of a sequence-structure family. *Curr Opin Struct Biol* **6**, 395-401 (1996).

22. Silengo, M., Del Monaco, A., Linari, A. & Lala, R. Low birth-weight, microcephalic malformation syndrome in a 46,XX girl and her 46,XY sister with agonadism: third report of the Kennerknecht syndrome or autosomal recessive Seckel-like syndrome with previously undescribed genital anomalies. *Am J Med Genet* **101**, 275-278 (2001).

23. Besse, A., Campos, A.D., Webster, W.K. & Darnay, B.G. TRAF-interacting protein (TRIP) is a RING-dependent ubiquitin ligase. *Biochem Biophys Res Commun* **359**, 660-664 (2007).

24. Lee, S.Y., Lee, S.Y. & Choi, Y. TRAF-interacting protein (TRIP): a novel component of the tumor necrosis factor receptor (TNFR)- and CD30-TRAF signaling complexes that inhibits TRAF2-mediated NF-kappaB activation. *J Exp Med* **185**, 1275-1285 (1997).

25. Zhang, M. *et al.* TRAF-interacting protein (TRIP) negatively regulates IFN-beta production and antiviral response by promoting proteasomal degradation of TANK-binding kinase 1. *J Exp Med* **209**, 1703-1711 (2012).

26. Park, E.S. *et al.* Early embryonic lethality caused by targeted disruption of the TRAF-interacting protein (TRIP) gene. *Biochem Biophys Res Commun* **363**, 971-977 (2007).

27. Raschle, M. *et al.* DNA repair. Proteomics reveals dynamic assembly of repair complexes during bypass of DNA cross-links. *Science* **348**, 1253671 (2015).

28. Han, C. *et al.* Cdt2-mediated XPG degradation promotes gap-filling DNA synthesis in nucleotide excision repair. *Cell Cycle* **14**, 1103-1115 (2015).

29. Almeida, S., Ryser, S., Obarzanek-Fojt, M., Hohl, D. & Huber, M. The TRAF-interacting protein (TRIP) is a regulator of keratinocyte proliferation. *J Invest Dermatol* **131**, 349-357 (2011).

30. Branzei, D. & Foiani, M. Maintaining genome stability at the replication fork. *Nat Rev Mol Cell Biol* **11**, 208-219 (2010).

31. Wallace, H.A. *et al.* TRIP/NOPO E3 ubiquitin ligase promotes ubiquitylation of DNA polymerase eta. *Development* **141**, 1332-1341 (2014).

32. Bienko, M. *et al.* Regulation of translesion synthesis DNA polymerase eta by monoubiquitination. *Mol Cell* **37**, 396-407 (2010).

33. Lehmann, A.R., McGibbon, D. & Stefanini, M. Xeroderma pigmentosum. *Orphanet J Rare Dis* **6**, 70 (2011).

34. Masutani, C. *et al.* The XPV (xeroderma pigmentosum variant) gene encodes human DNA polymerase eta. *Nature* **399**, 700-704 (1999).

35. Johnson, R.E., Kondratick, C.M., Prakash, S. & Prakash, L. hRAD30 mutations in the variant form of xeroderma pigmentosum. *Science* **285**, 263-265 (1999).

36. Despras, E., Daboussi, F., Hyrien, O., Marheineke, K. & Kannouche, P.L. ATR/Chk1 pathway is essential for resumption of DNA synthesis and cell survival in UV-irradiated XP variant cells. *Hum Mol Genet* **19**, 1690-1701 (2010).

37. Shi, W. *et al.* The role of RPA2 phosphorylation in homologous recombination in response to replication arrest. *Carcinogenesis* **31**, 994-1002 (2010).

38. Nakada, S., Chen, G.I., Gingras, A.C. & Durocher, D. PP4 is a gamma H2AX phosphatase required for recovery from the DNA damage checkpoint. *EMBO Rep* **9**, 1019-1026 (2008).

39. Chowdhury, D. *et al.* A PP4-phosphatase complex dephosphorylates gamma-H2AX generated during DNA replication. *Mol Cell* **31**, 33-46 (2008).

40. Chowdhury, D. *et al.* gamma-H2AX dephosphorylation by protein phosphatase 2A facilitates DNA double-strand break repair. *Mol Cell* **20**, 801-809 (2005).

41. Feng, J. *et al.* Protein phosphatase 2A-dependent dephosphorylation of replication protein A is required for the repair of DNA breaks induced by replication stress. *Mol Cell Biol* **29**, 5696-5709 (2009).

42. Taylor, S.S. & McKeon, F. Kinetochore localization of murine Bub1 is required for normal mitotic timing and checkpoint response to spindle damage. *Cell* **89**, 727-735 (1997).

43. Soria, G., Polo, S.E. & Almouzni, G. Prime, repair, restore: the active role of chromatin in the DNA damage response. *Mol Cell* **46**, 722-734 (2012).

44. Lancaster, M.A. & Knoblich, J.A. Spindle orientation in mammalian cerebral cortical development. *Curr Opin Neurobiol* **22**, 737-746 (2012).

45. Lessel, D. *et al.* Mutations in SPRTN cause early onset hepatocellular carcinoma, genomic instability and progeroid features. *Nat Genet* **46**, 1239-1244 (2014).

46. Conlon, I. & Raff, M. Size control in animal development. *Cell* **96**, 235-244 (1999).

47. Bicknell, L.S. *et al.* Mutations in the pre-replication complex cause Meier-Gorlin syndrome. *Nat Genet* **43**, 356-359 (2011).

48. Bicknell, L.S. *et al.* Mutations in ORC1, encoding the largest subunit of the origin recognition complex, cause microcephalic primordial dwarfism resembling Meier-Gorlin syndrome. *Nat Genet* **43**, 350-355 (2011).

49. Guernsey, D.L. *et al.* Mutations in origin recognition complex gene ORC4 cause Meier-Gorlin syndrome. *Nat Genet* **43**, 360-364 (2011).

50. Murga, M. *et al.* A mouse model of ATR-Seckel shows embryonic replicative stress and accelerated aging. *Nat Genet* **41**, 891-898 (2009).

51. Cooke, M.S., Evans, M.D., Dizdaroglu, M. & Lunec, J. Oxidative DNA damage: mechanisms, mutation, and disease. *FASEB J* **17**, 1195-1214 (2003).

52. Langevin, F., Crossan, G.P., Rosado, I.V., Arends, M.J. & Patel, K.J. Fancd2 counteracts the toxic effects of naturally produced aldehydes in mice. *Nature* **475**, 53-58 (2011).

53. Frank, K.M. *et al.* DNA ligase IV deficiency in mice leads to defective neurogenesis and embryonic lethality via the p53 pathway. *Mol Cell* **5**, 993-1002 (2000).

FIGURE LEGENDS

Figure 1. Mutations in *TRAIP* cause primordial dwarfism

(**a**) Mutations identified in *TRAIP*. Top, schematic of *TRAIP* gene structure; middle, TRAIP protein structure; bottom, sequence electropherograms demonstrating (middle, right panels) homozygous nonsense mutations in Patient 1 (P1) and Patient 2 (P2) and (left) a homozygous missense mutation, Arg18Cys in Patient 3 (P3). (**b**) A physiochemically similar residue is present at codon 18 in all vertebrates. Sequence alignments of *Homo sapiens, Pan troglodytes, Mus musculus, Gallus gallus, Xenopus tropicalis* and *Danio rerio* using Clustal W. (**c**) Patients with TRAIP mutations have prenatal onset severe growth failure with disproportionate microcephaly. Birth weight (BWGT), current height (HGT) and current head circumference (OFC) plotted as z-scores (standard deviations from population mean for age and sex). 97.5% of general population will lie above the dashed line at –2 S.D. Black bars indicate mean values. (**d**) Cerebral cortical size is markedly reduced with simplification of gyral folding. MRI T2-weighted sagittal and axial images of P3 (age 3 years) compared with control scans of a healthy child (age 3 years 1 month). Scale bar, 2 cm. (**e**) Photographs of affected individuals with *TRAIP* mutations demonstrating facial similarities, including an elongated narrow face and micrognathia. Informed consent to publish photographs was obtained from families.

Figure 2. TRAIP mutations result in reduced cellular levels of TRAIP protein

(**a**) The Arg185* mutation severely reduces *TRAIP* transcript levels in P1 and P2 patient cell lines. RT-PCR using primers in 5' and 3' UTR to amplify *TRAIP* transcripts in primary fibroblasts and lymphoblastoid cell lines (LCLs) demonstrates marked decrease in full length *TRAIP* transcript, consistent with nonsense-mediated decay. Additional low intensity PCR products are evident, that represent alternatively spliced transcripts, confirmed by subcloning and Sanger sequencing (lower panels). These include transcripts, which through omission of exon 7, or exons 6, 7 and 8, retain an open reading frame and result in protein products with small internal deletions. Loading control, *GAPDH*. (**b**) TRAIP protein levels are reduced in patients with Arg185* and the Arg18Cys mutations. Immunoblotting with an affinity purified rabbit anti-TRAIP antibody raised against recombinant TRAIP protein demonstrates reduced levels of the 53 kDa TRAIP protein in P3, and marked depletion in P1 and P2 where protein is only detectable on prolonged exposure (**Supplementary Fig. 2**). Loading controls, actin and vinculin.

Figure 3. TRAIP localizes to sites of UV-induced DNA damage

(**a**) TRAIP localizes to DNA damage sites induced by UV laser microirradiation both in the absence and presence of pre-treatment with BrdU as a damage sensitizer. Representative images, before and after UV laser microirradiation. Scale bar, 5 μm. (**b**) GFP-TRAIP colocalizes with γH2AX and with RFP-PCNA at sites of UV laser-induced damage. Representative images of UV laser-irradiated GFP-TRAIP expressing cells immunostained for γH2AX (pre-sensitized with BrdU) or co-expressing RFP-PCNA (no BrdU pre-treatment) as indicated. Scale bar, 5 μm. (**c**, **d**) GFP-TRAIP is detected by a Proximity Ligation Assay (PLA) in close proximity to PCNA, an association enhanced after UV-induced damage. (**c**) Representative images of PLA signals/nucleus in doxycycline-inducible GFP-TRAIP HeLa cells before and after damage with 25 J/m^2 UV-C. Scale bar, 5 μm. (**d**) Quantification of PLA signals/nucleus. Box plots, center line denote mean values, box 25/75 %, whiskers 5/95 %, data pooled from n=2 independent experiments, n>65 data points per condition per experiment; Mann Whitney rank sum test: *** p<0.001. (**e**) TRAIP accumulates at sites of localized UV damage, colocalising with RPA and γH2AX. Representative immunofluorescence images of MRC5 cells transfected with GFP-TRAIP or GFP alone after UV-C irradiation through 3 μm microfilters. Scale bar, 5 μm.

Figure 4. TRAIP is required for UV-induced RPA2 and H2AX phosphorylation during S-phase

(**a**) Phosphorylation of downstream ATR substrates is unaffected by TRAIP depletion. HeLa cells were transfected with RNAi against TRAIP or luciferase (control). After 72h, cells were UV-C treated, before harvesting at indicated times. Cell lysates were analyzed by Western blot as indicated. (**b**, **c**) TRAIP loss reduces RPA2 phosphorylation and histone H2AX phosphorylation (γH2AX) in response to UV. HeLa cells transfected with TRAIP and control siRNAs (**b**) or primary patient fibroblasts (**c**) were UV-C treated, harvested and immunoblotted as indicated. (**d**, **e**) Quantification of pS4/S8-RPA2 (**d**) and γH2AX (**e**) in primary fibroblasts after UV. Chemiluminescence from Western blots quantified using ImageQuant. Mean ± SEM, n=3 experiments; values normalized to total RPA2 signal; two-way ANOVA across all time points: *** p<0.001, ** p<0.01. (**f**) Retroviral complementation with wild-type TRAIP rescues impaired phosphorylation of RPA2 and H2AX after UV-C irradiation in TRAIP^{Arg185*} cells. Fibroblasts derived from P2^{Arg185*} were immortalized with hTERT, denoted P2^{TERT}; and reconstituted with pMSCV-TRAIP, P2$^{TERT+TRAIP}$. (**g**) TRAIP is required for optimal RPA2 and H2AX phosphorylation in S-phase. P2^{TERT} and P2$^{TERT+TRAIP}$ cells were irradiated with 15 J/m^2 UV-C, labeled with EdU for 4 h, pre-extracted, fixed and co-stained for pS4/S8-RPA2 or γH2AX, EdU and DAPI. Representative images of immunofluorescence staining of pS4/S8-RPA2 (left), quantification of pS4/S8-RPA2 (middle) and γH2AX (right) signal integrated density in EdU-positive and EdU-negative

cells. Mean ± SEM for n=3 experiments, values normalized to $P2^{TERT+TRAIP}$; Student's *t*-test: *p<0.05; ***p<0.001. Scale bar, 10 μm.

Figure 5. Impaired growth and cell cycle progression in TRAIP deficient cells

(**a**) TRAIP mutations impair cell proliferation. Cell numbers of passage-matched primary fibroblast cell lines derived from patients or controls were determined over 17 days to establish growth rates. Mean ± SEM for n=3 experiments; fold growth relative to day 0. (**b**) Complementation with wild-type TRAIP rescues the slow growth phenotype of $TRAIP^{Arg185*}$ cells. $P2^{TERT}$ fibroblasts were reconstituted with pMSCV-vector only or pMSCV-TRAIP. Growth rates of passage-matched cell lines were analyzed over 18 days. Mean ± SEM for n=3 experiments; fold growth relative to day 0. (**c**) Doubling times of fibroblast cells from (**a**) and (**b**). Mean ± SEM for n=3 experiments; Student's *t*-test: *p<0.05; **p<0.01. (**d**) TRAIP-depleted cells exhibit delayed S/G2 phase progression. HeLa cells were transfected with RNAi against TRAIP or luciferase (Luc) control. 72h later cells were pulse labeled with 10 μM BrdU for 30 min before washing out and replacing with fresh media. At indicated times, cells were harvested, fixed and prepared for flow cytometry. Left, Western blots of RNAi for TRAIP or control Luc demonstrate effective TRAIP depletion. Middle, representative images of gating used in analysis of flow cytometry data. Right, quantification of the relative number of cells with 4n content; fold change relative to 0h. Mean ± SEM, n=4 experiments. Fold change relative to 0h; two-way ANOVA across all time points: ** p<0.01.

Figure 6. Replication fork stalling is increased following UV-induced DNA damage in TRAIP patient cells

(**a**) First label termination events (representing elevated replication fork stalling) are increased after UV irradiation in TRAIP patient fibroblasts. Top left panel, schematic of the experimental plan. Bottom left panel, representative images of ongoing or stalled replication forks and new origin firing from DNA fiber spreads of primary fibroblasts. Right panel, quantification of ongoing forks, 2^{nd} label only (new origin firing) and 1^{st} label termination (fork stalling) structures in fibroblast cells. Mean ± SD, n=3 independent experiments, >400 structures per cell line per experiment quantified. Student's *t*-test: *p<0.05; **p<0.01; ns, not significant. (**b**, **c**) Substantial fork asymmetry is seen in UV-treated patient cells. (**b**) Representative images of DNA fibers from controls (Con1, Con2) and patient fibroblasts (P2, P3) after 30 J/m^2 UV treatment. (**c**) Quantification of replication fork asymmetry. Ratio of left/right fork length; mean ratio for each cell line is indicated in italics; Mann Whitney Rank sum test: ***p<0.001; ns, not significant. Data points pooled from n=2 independent experiments, >50 structures per cell line per experiment quantified.

Table 1. Clinical summary of individuals with *TRAIP* mutations

Individual	Gender	Consanguinity	Ancestry	Nucleotide mutation	Protein alteration	Gestation (weeks)	BWT (kg) *SD*	Age (years)	Height (cm) *SD*	OFC (cm) *SD*	Karyotype	Craniofacial features	Clinical synopsis
P1	F	NC	Italian	c.553C>T	p.Arg185*	37	1.95 *-2.7*	5	85.9 *-5.4*	44 *-6.5*	46, XX	Microcephaly, scaphocephaly, long narrow face, micrognathia.	IUGR; recurrent severe lower respiratory tract infections; delayed speech, 2 deceased siblings with similar phenotypes.
P2	M	NC	English	c.553C>T	p.Arg185*	32	1.2 *-2.2*	7	103.5 *-3.9*	40.7 *-8.3*	46, XY	Microcephaly, scaphocephaly, long narrow face, micrognathia.	IUGR; recurrent severe lower respiratory tract infections; moderate global developmental delay; hypertrichosis.
P3	M	3rd cousin	Turkish	c.52C>T	p.Arg18Cys	40	1.75 *-2.9*	3	80 *-4.6*	40.1 *-8.1*	46, XY	Microcephaly, long narrow face, micrognathia.	IUGR; asthma; mild global developmental delay.

All parents were demonstrated to be heterozygote carriers of the mutations identified, confirming appropriate segregation within the family. Age is shown in years at time of measurements. BWT, birth weight; SD, standard deviation from the population mean for age and sex; OFC, occipital frontal circumference; F, female; M, male; NC, non-consanguineous; IUGR, intrauterine growth restriction.

ONLINE METHODS

Research subjects

Genomic DNA from the affected children and family members was extracted from peripheral blood using standard methods or saliva samples using Oragene collection kits according to the manufacturer's instructions. Informed consent was obtained from all participating families and the studies were approved by the ethics review boards, the Scottish Multicentre Research Ethics Committee (04:MRE00/19) and the Ethics Committee of the University Hospital Cologne, Germany. Parents provided written consent for the publication of photographs of the affected individuals.

Exome sequencing and haplotype analysis

Exome sequencing of genomic DNA and variant filtering was performed as described previously[54,55]. Cohort resequencing was performed by Sanger sequencing of PCR products representing all coding exons of TRAIP (primer sequences available on request), with variant calling using MutationSurveyor (SoftGenetics Inc). Haplotype analysis was undertaken by SNP genotyping both patients using Affymetrix CytoScan 750K arrays. Genotypes were generated using Affymetrix Genotyping Console software and examined manually.

Inbreeding coefficients for P1 and P2 were estimated using FEstim[20], using SNP genotypes with confidence scores < 10^{-4}, after linkage disequilibrium (LD) pruning using PLINK v1.90b3o (64-bit) [56]. Runs of homozygosity (ROH) were also used to calculate F_{ROH} using PLINK, as described previously[57,58]. In brief, SNPs were excluded with NoCall frequency above 3% across individuals or with a minor allele frequency (MAF) < 5%. ROH were defined as runs of at least 50 consecutive homozygous SNPs spanning at least 1.5 Mb, with less than a 1 Mb gap between adjacent ROHs and a density of SNP coverage within the ROH of no more than 50 Kb/SNP, with at most one heterozygous SNP and five NoCalls allowed per window.

Cell culture

Lymphoblastoid cell lines (LCLs) were maintained in RPMI 1640 supplemented with 15% fetal bovine serum, L-glutamine and penicillin/streptomycin antibiotics in 5% CO_2 and normoxic conditions. Lymphoblastoid cell lines were generated in house from peripheral blood samples by EBV transformation using standard methods. Dermal primary fibroblasts were grown from skin punch biopsies in AmnioMax medium (Life Technologies) and then maintained in Dulbecco's MEM (modified Eagle's medium; DMEM) supplemented with 10% fetal bovine serum, 5% L-glutamine and 5% penicillin/streptomycin antibiotics in 5% CO_2 and hypoxic 3% O_2 conditions. Patient cell lines

were validated using Sanger sequencing and immunoblotting. HeLa cells were maintained in DMEM supplemented with 10% fetal bovine serum, 5% L-glutamine and 5% penicillin/streptomycin antibiotics in 5% CO_2 and normoxic conditions. HeLa (ATCC), U2OS and MRC5 (GDSC, Sussex) cells were cultured in DMEM supplemented with 10% fetal bovine serum, 5% L-glutamine and 5% penicillin/streptomycin antibiotics.

Stable cell lines were generated by Flp recombinase-mediated integration using HeLa-Flp-In T-REx host cells (gift from Stephen Taylor, University of Manchester[42]) transfected with pcDNA5/FRT/TO-EGFP (vector only or EGFP-TRAIP) and pCAGGS-Flp.e (gift from Dirk-Jan Kleinjan, University of Edinburgh). Transfected cells were selected using 5 μg/ml blasticidin and 400 μg/ml hygromycin and the resulting colonies were then expanded for testing. Protein expression was induced with 1 μg/ml tetracycline treatment. HeLa cells expressing RFP-PCNA were a gift from Agata Lichawska and Jörg Mansfeld, Gurdon Institute. Primary fibroblasts derived from P2 were immortalized with hTERT retroviral supernatant with 4 μg/ml polybrene and infected with pMSCV-vector only or pMSCV-TRAIP. Selection was performed using 750 ng/ml puromycin and 500 μg/ml neomycin. Expression of the protein was verified by Western blot (**Supplementary Fig. 6c**). All cell lines were routinely tested for mycoplasma.

Cell treatments

Plasmids and siRNA oligos were transfected in Opti-MEM reduced serum media using Oligofectamine (Life Technologies) according to the manufacturer's guidelines. The siRNA oligonucleotide sequences are listed in Supplementary Table 1a. Where indicated, cells were treated with 10 μM MG132 (Cayman Chemicals), 10 or 15 J/m^2 UV-C, 2 mM hydroxyurea (Sigma-Aldrich), 0.5 μM aphidicolin (Sigma-Aldrich), 50 ng/ml mitomycin C (Sigma-Aldrich) or 2 mM thymidine (Sigma-Aldrich).

RT-PCR

Total RNA was extracted from cell lines using the RNeasy kit (Qiagen) according to the manufacturer's instructions. DNA was removed by treatment with DNase I (Qiagen) and cDNA was generated using random oligomer primers and AMV RT (Roche). The RT-PCR primer pairs used are listed in Supplementary Table 1b.

Western blot analysis and antibodies

Whole cell extracts were obtained by lysis and sonication of cells in UTB buffer (8 M Urea, 50 mM Tris pH 7.5, 150 mM β-mercaptoethanol, protease inhibitor cocktail (Roche)) or in NP-40 lysis buffer

(50 mM Tris pH 8.0, 280 mM NaCl, 0.5% NP-40, 0.2 mM EDTA, 0.2 mM EGTA, 10% Glycerol, 1 mM DTT, protease inhibitor cocktail (Roche), 1 mM PMSF, phosphatase inhibitors (40 mM NaF, 1 mM sodium orthovanadate)) and analyzed by SDS-PAGE following standard procedures. Protein samples were run on 6-12% acrylamide SDS-PAGE or 4-12% NuPage mini-gels (Life Technologies) and transferred onto nitrocellulose membrane. Immunoblotting was performed using antibodies to RPA2 (Santa Cruz, sc-28709; 1:1000), pS4/S8-RPA2 (Bethyl Laboratories, A300-245A; 1:1000), pS33-RPA2 (Bethyl Laboratories, A300-246A; 1:1000), H2A (Millipore, 07-146; 1:5000), γH2AX (Millipore, 05-636; 1:1000), actin (Sigma-Aldrich, A2066; 1:5000), vinculin (Sigma-Aldrich, V9264; 1:1000), pS966-SMC1 (Bethyl Laboratories, A300-050A; 1:1000), SMC1 (Abcam, ab9262; 1:2000), pS343-NBS1 (Cell Signaling Technology, 3001; 1:500), NBS1 (Oncogene, PC269T; 1:500), pS345-CHK1 (Cell Signaling Technology, 2341; 1:500), CHK1 (Santa Cruz, sc-8408; 1:1000), pT68-CHK2 (Cell Signaling, 2661; 1:500) , CHK2 (Santa Cruz, sc-9064; 1:500), pS1981-ATM (Cell Signaling, 4526; 1:500), ATM (Abcam, ab31842; 1:1000), pS2056-DNA-PKcs (Abcam, ab18192; 1:400), DNA-PKcs (Abcam, ab32566; 1:1000), pS824-KAP1 (Bethyl Laboratories, A300-767A; 1:5000), KAP1 (Bethyl Laboratories, A300-274A; 1:10000), CDK1 (Sigma-Aldrich, P7962; 1:1000), cyclin A (Santa Cruz, sc-751; 1:1000), cyclin B1 (Cell Signaling Technology, 4135; 1:1000), pS10-Histone H3 (Millipore, 06-570; 1:1000), Histone H3 (Millipore, 07-690; 1:10,000), FLAG (Agilent, clone M2; 1:1000).
TRAIP antibody was generated from recombinant TRAIP protein using pGEX-4T-2-TRIP-N (gift from Robert Geahlen, Purdue University, USA). Antibody was affinity purified from rabbit sera (Eurogentec) and specificity established using patient cell lysates and RNAi.

Laser line assay

Laser micro-irradiation and live cell imaging were performed as described previously in supplemental methods of ref[59]. Plasmids were transfected into U2OS cells using *Trans*IT-LT1 (Mirus Bio), according to the manufacturer's instructions. Images were acquired using an Olympus FluoView 1000 confocal microscope.

Immunofluorescence: GFP-TRAIP localisation

MRC5 fibroblasts were transfected with EGFP-TRAIP using Lipofectamine 2000 (Life Technologies) according to the manufacturer's instructions. The cells were trypsinised and seeded onto coverslips 6 hours post-transfection. The following day, the cells were washed once in warm PBS and treated with 2 mM hydroxyurea for 24 h or irradiated either at 25 J/m^2 for global UV-C irradiation (fluency rate 0.8 J/m^2/s) or at 120 J/m^2 for local UV-C irradiation through isopore membrane 3 μM filters (Millipore) and fixed 1 h or 1.5 h post UV-C, respectively. Immunofluorescence (IF) was performed as

previously described[60] with minor modifications. Briefly, the cells were either pre-extracted in CSK100 buffer and then fixed in 4% paraformaldehyde for 15 min at room temperature or fixed first and then permeabilized in 0.5% Triton-X100 in PBS at room temperature for 15 min. Primary and secondary antibodies' incubations were performed in IF buffer (3% BSA in PBS) for 1 hour at room temperature. Primary antibodies: XPC (Santa Cruz, 1:100), PCNA (PC10, Santa Cruz, 1:400), γH2AX (Millipore, 1:500), RPA2 (Calbiochem, 1:200); secondary antibodies: Alexa Fluor-594 or Alexa Fluor-488 (Molecular Probes); DAPI 0.4 μg/ml (Vectashield). For EdU detection, cells were pulsed with 20 μM EdU for 20 min and then detected using the Click-iT EdU Imaging kit (Life Technologies) according to the manufacturer's protocol. Fluorescence images were taken using a Nikon E600 Eclipse microscope equipped with a 60X oil lens, and images were acquired and analysed using Volocity Software v4.1 (Improvision).

Proximity ligation assay (PLA)

Cells from stable EGFP/ EGFP-TRAIP HeLa Flp-In T-REx cell lines were fixed with methanol at -20 °C for 10 min followed by a 5 min extraction in 0.3% Triton-X100 in PBS. Cells were then incubated in anti-PCNA antibody (Santa Cruz, PC10; 1:500) and anti-GFP antibody (Abcam, ab6556; 1:500), and *in situ* proximity ligation was performed using a Duolink Detection Kit in combination with anti-Mouse PLUS and anti-Rabbit MINUS PLA Probes, according to the manufacturer's instructions (Sigma Aldrich Duolink). Nuclear foci were imaged using a Nikon E600 Eclipse microscope equipped with a 60X oil lens, and images were acquired and analysed using Volocity Software v4.1 (Improvision). The number of nuclear foci/cell was quantified using ImageJ. More than 50 cells were analyzed per experiment per condition.

Quantitative immunofluorescence of pSer4/Ser8-RPA2 and γH2AX

Passage-matched TERT-immortalized fibroblasts were seeded on coverslips, 24 h later damaged with 15 J/m2 UV-C irradiation and left to recover for 4 hours in media containing 10 μM EdU. To remove soluble proteins prior to immunofluorescence, cells were pre-extracted for 10 min on ice with ice-cold buffer (25 mM Hepes 7.4, 50 mM NaCl, 1mM EDTA, 3 mM $MgCl_2$, 300 mM sucrose and 0.5% TritonX-100) and then fixed with 4% paraformaldehyde for 15 min. EdU immunolabeling was performed using Click-iT EdU Imaging Kit (Invitrogen, C10337) according to the manufacturer's protocol. Afterwards cells were stained for pS4/S8-RPA2 (Bethyl Laboratories, A300-245A; 1:1000) or γH2AX (Millipore, 05-636; 1:800) and then stained with secondary antibodies conjugated to Alexa Fluor-568 (Life Technologies) and DAPI. For quantification of signal integrated densities, images were visualized using a Zeiss Axioplan 2 microscope with iVision software (BioVision Technologies) and

captured using 40X oil-immersion objective. Exposure time, binning, microscope settings and light source intensity were kept constant for all the samples. Nuclei were segmented on the basis of DAPI staining and then signal integrated density of pS4/S8-RPA2 and γH2AX staining quantified for each nuclear region using ImageJ software (US National Institutes of Health). More than 50 EdU positive and 150 EdU negative cells were analyzed per experiment per condition.

Comet assay

Neutral comet assays were carried out using the Trevigen Comet Assay™ electrophoresis kit (4250-050-K) according to manufacturer's instructions. Briefly, $1x10^5$ primary fibroblasts were seeded in 6 well plates overnight for approximately 16 hours. Cells were then treated with 15 J/m^2 UV-C and allowed to recover for 4 hours in media. Cells were collected and embedded into low melting agarose on 'comet' slides (Trevigen) and incubated in lysis solution overnight in the dark at 4°C. Cells were then electrophoresed in buffer (50 mM Tris pH 9.0, 150 mM sodium acetate) for 45 min at 21 volts at 4°C in the dark. Comet slides were immersed in DNA precipitation solution (1 M ammonium acetate, 95% ethanol) for 30 min and 70% ethanol for 30 min at room temperature and dried at 37°C for 15 min. Slides were stained in 1x SYBR gold in TE buffer (pH 7.5) for 30 min at room temperature, dried for an additional 15 min at 37°C and then visualized with an epifluorescence microscope and analyzed using CaspLab software.

FACS analysis

Passage-matched TERT-immortalized fibroblasts grown in AmnioMax medium (Life Technologies) or HeLa cells were pulse labeled with 10 µM BrdU for 30 min before fixation with 70% ethanol at -20°C for 16 h. Cells were then digested with 1 mg/ml pepsin and denatured with 2 M HCl, before washing with PBS and blocking in 0.5% BSA, 0.5% Tween-20. BrdU labeling was detected using anti-BrdU antibody (Abcam, ab6326; 1:75) and FITC-conjugated anti-rat secondary antibody. DNA content was assessed by staining with 50 µg/ml propidium iodide. Cells were sorted on a BD Biosciences FACS Aria II and data were analyzed using FlowJo software (v7.6.1, Tree Star).

Mitotic index of pulse labeled EdU cells

HeLa cells were seeded on poly-L-lysine-coated coverslips 48 h after siRNA transfection. The following day, 10 µM EdU was added to the cells for 30 min, washed out with PBS and media replaced. 6 h later cells were fixed using 4% paraformaldehyde and stained for pSer10-Histone H3 (Cell Signalling, 9706; 1:250) and EdU (Click-iT EdU Imaging Kit, Invitrogen, C10337) according to the manufacturer's protocol. Cells were then stained with secondary antibody conjugated to Alexa

Fluor-568 (Life Technologies) and analyzed using a Zeiss Axioplan 2 microscope equipped with a 60X oil-immersion objectives and iVision software (BioVision Technologies).

G2/M checkpoint assay

A previously established assay was used to determine mitotic cell number after damage-induced checkpoint activation[61]. In brief, HeLa cells transfected with RNAi against TRAIP or luciferase (control) for 72 h were treated with 10 J/m^2 UV-C and fixed in 96% ethanol 4 h later. Mitotic cells were determined by pSer10-Histone H3 (Cell Signalling, 9706; 1:250) staining and flow cytometry on a BD Biosciences FACS Aria II.

DNA fiber spreading assay

Passage-matched primary or TERT-immortalized fibroblasts were pulse labeled with CldU for 20 min, washed with PBS and damaged with 30 J/m^2 UV-C, 2 mM hydroxyurea for 2 h or 0.5 µM aphidicolin before being pulse labeled with IdU for 20 or 40 min as indicated. 0.5 µM aphidicolin was added to the cells for 40 min together with IdU pulse labeling. 50 ng/ml mitomycin C was added to the cells for 24 h before CldU pulse labeling and left on during 20 min CldU and 20 min ldU pulse labeling. Cells were harvested by trypsinization and cell pellets were washed in PBS. 5x10^5 cells were lysed directly onto glass slides using spreading buffer (200 mM Tris-HCl pH 7.5, 50 mM EDTA, 0.5% SDS) and fixed in methanol:acetic acid (3:1 ratio). Following 2.5 M HCl denaturation, CldU was detected using rat anti-BrdU (clone BU1/75, ICR1; Abcam, ab6326; 1:750) and IdU was detected using mouse anti-BrdU (clone B44; BD Biosciences, 347583; 1:750). Slides were then fixed in 4% paraformaldehyde before immunostaining with secondary antibodies conjugated to Alexa Fluor-594 or Alexa Fluor-488 (Life Technologies). Labeled DNA fibers were visualized using a Zeiss Axioplan 2 microscope with iVision software (BioVision Technologies). Images were captured using 40X oil-immersion objectives and analyzed using ImageJ software (US National Institutes of Health).

In vitro transcription/translation

The TnT® T7 Quick Coupled Transcription/Translation System (Promega) was used to produce FLAG-tagged TRAIP (WT, R18C or R185X) *in vitro* following the manufacturer's instructions. Briefly, 250 ng of plasmid DNA (pcDNA-based, TRAIP with an N-terminal single FLAG epitope) in 2.25 µl of water was mixed with 10 µl TNT® T7 Quick Master Mix, 0.25 µl of 1 mM methionine and incubated for 90 min at 30°C. For immunoblotting 1 µl of each reaction was separated by SDS-PAGE on 4-12% NuPAGE gels (Life Technologies), and TRAIP was detected using anti-FLAG or anti-TRAIP antibodies.

Statistical analysis

Numerical data were analyzed using parametric and nonparametric statistical tests, namely Student's *t*-test, ANOVA or Mann Whitney Rank sum test, as indicated. Statistical tests were two-sided unless otherwise stated in figure legend. Significance thresholds are indicated in figure legends.

METHODS-ONLY REFERENCES

54. Martin, C.A. *et al.* Mutations in PLK4, encoding a master regulator of centriole biogenesis, cause microcephaly, growth failure and retinopathy. *Nat Genet* **46**, 1283-1292 (2014).

55. Keupp, K. *et al.* Mutations in WNT1 cause different forms of bone fragility. *Am J Hum Genet* **92**, 565-574 (2013).

56. Purcell, S. *et al.* PLINK: a tool set for whole-genome association and population-based linkage analyses. *Am J Hum Genet* **81**, 559-575 (2007).

57. Joshi, P.K. *et al.* Directional dominance on stature and cognition in diverse human populations. *Nature* **523**, 459-462 (2015).

58. McQuillan, R. *et al.* Runs of homozygosity in European populations. *Am J Hum Genet* **83**, 359-372 (2008).

59. Polo, S.E. *et al.* Regulation of DNA-end resection by hnRNPU-like proteins promotes DNA double-strand break signaling and repair. *Mol Cell* **45**, 505-516 (2012).

60. Despras, E., Delrieu, N., Garandeau, C., Ahmed-Seghir, S. & Kannouche, P.L. Regulation of the specialized DNA polymerase eta: revisiting the biological relevance of its PCNA- and ubiquitin-binding motifs. *Environ Mol Mutagen* **53**, 752-765 (2012).

61. Stewart, G.S., Wang, B., Bignell, C.R., Taylor, A.M. & Elledge, S.J. MDC1 is a mediator of the mammalian DNA damage checkpoint. *Nature* **421**, 961-966 (2003).

Figure 1

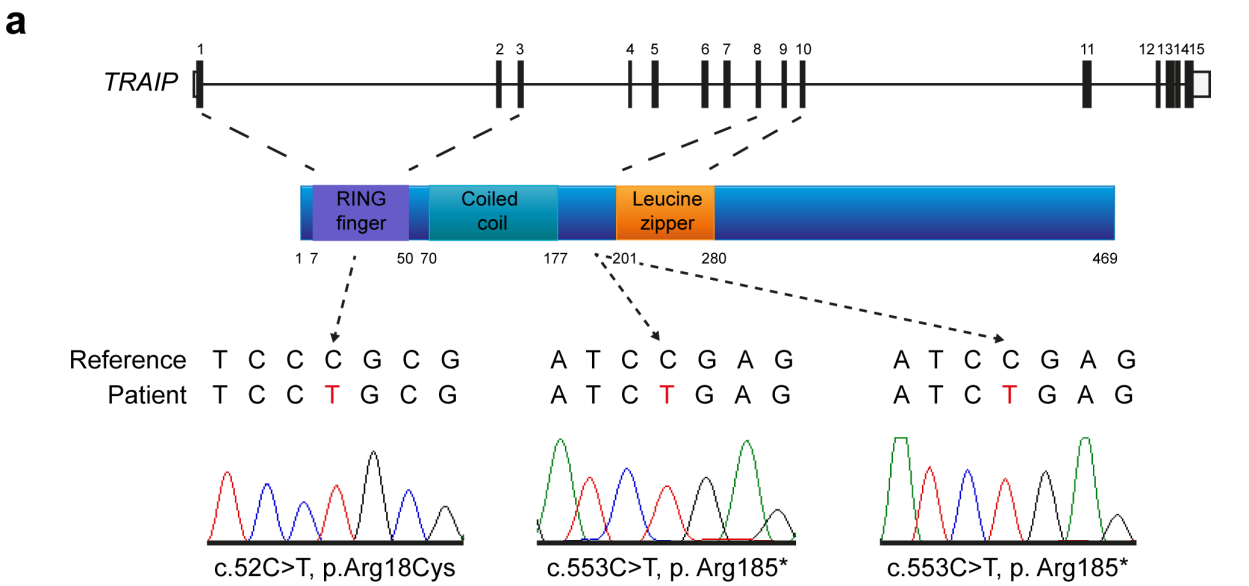
a
TRAIP
1
2 3
4 5
6 7
8
9 10
11
12 13 14 15
RING finger
Coiled coil
Leucine zipper
1 7
50 70
177
201
280
469
Reference T C C C G C G
Patient T C C T G C G
A T C C G A G
A T C T G A G
A T C C G A G
A T C T G A G
c.52C>T, p.Arg18Cys
c.553C>T, p. Arg185*
c.553C>T, p. Arg185*


b
H. sapiens 1 MPIRALCTICSDFFDHSRDVAAIHCGHTFHLQCLIQWFET 40
P. troglodytes 1 MPIRALCTICSDFFDHSRDVAAIHCGHTFHLQCLIQWFET 40
M. musculus 1 MPIRALCTICSDFFDHSRDVAAIHCGHTFHLQCLIQWFET 40
G. gallus 1 MPIRAHCTICSDFFDNARDVAAVPCGHTFHRACLFQWFDT 40
X. tropicalis 1 MPIRAYCTICSDFFDNSRDVAAVTCGHTFHQECLLQWFHS 40
D. rerio 1 MPIRAYCTICSDFFDNSKDVAAIHCGHTFHYSCLLQWFQS 40

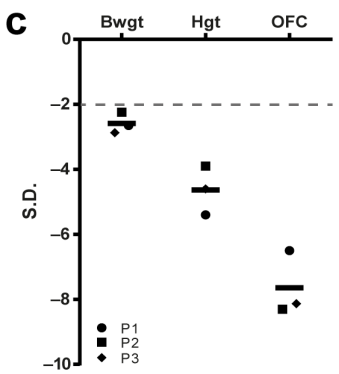
c
Bwgt
Hgt
OFC
0
−2
−4
−6
−8
−10
S.D.
P1
P2
P3

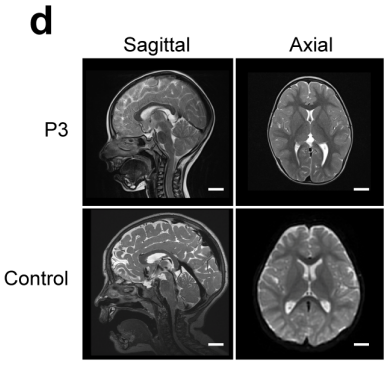
d
Sagittal
Axial
P3
Control

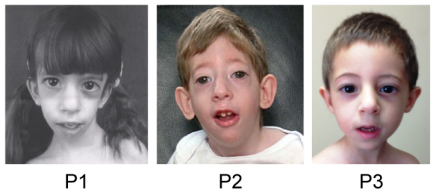
e
P1
P2
P3

Figure 2

a

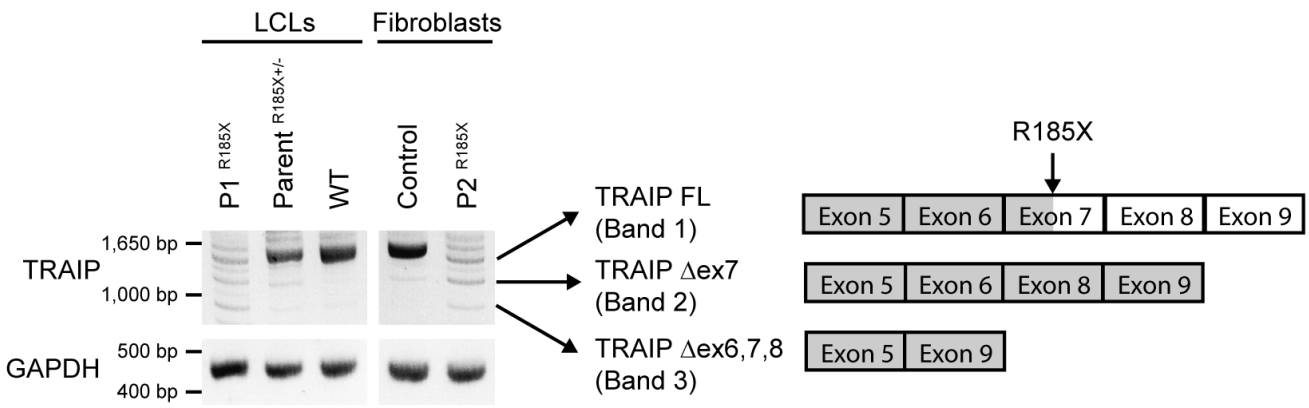

Normal splicing:

Band 1, full length:

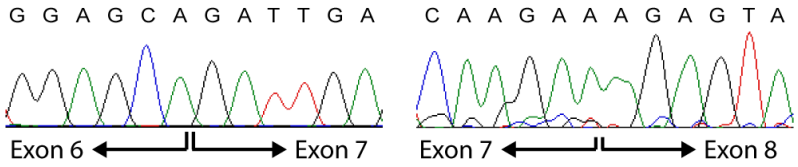

Band 1, full length:

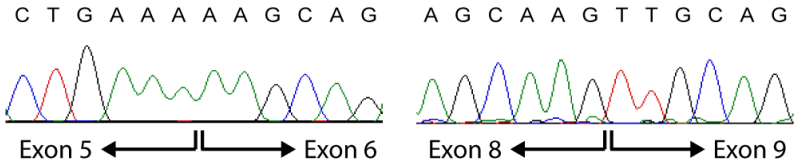

Additional splicing:

Band 2, exon 7 deleted:

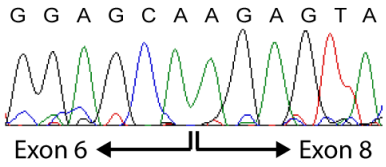

Band 3, exons 6, 7 and 8 deleted:

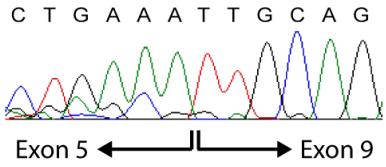

b

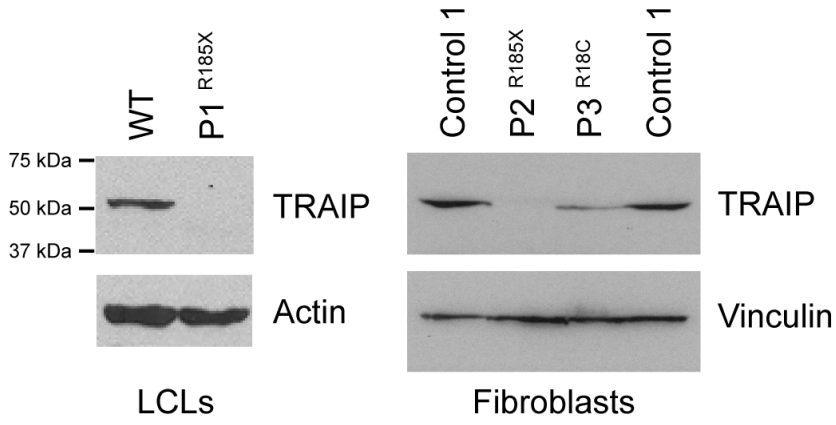

Figure 3

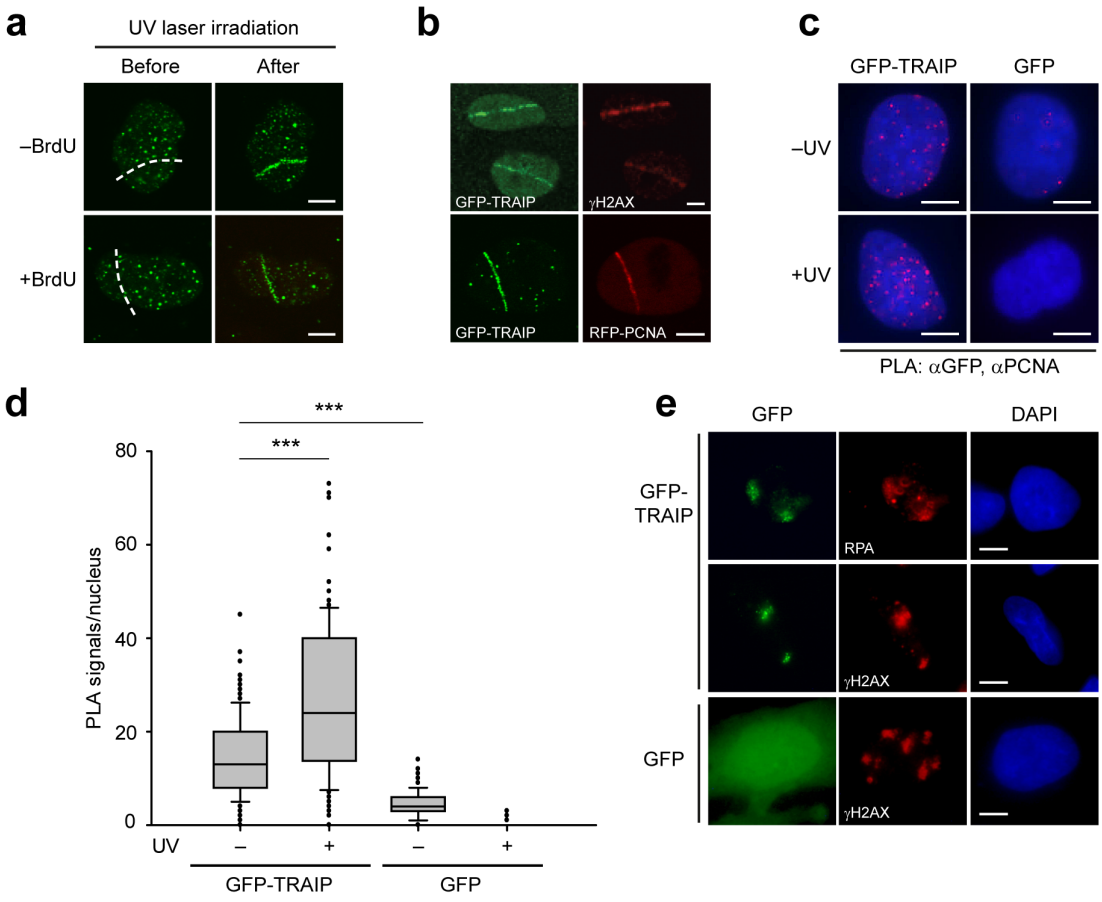
a
UV laser irradiation
Before
After
–BrdU
+BrdU
b
GFP-TRAIP
γH2AX
GFP-TRAIP
RFP-PCNA
c
GFP-TRAIP
GFP
–UV
+UV
PLA: αGFP, αPCNA
d
***
***
PLA signals/nucleus
80
60
40
20
0
UV
–
+
–
+
GFP-TRAIP
GFP
e
GFP
DAPI
GFP-TRAIP
RPA
γH2AX
GFP
γH2AX

Figure 4

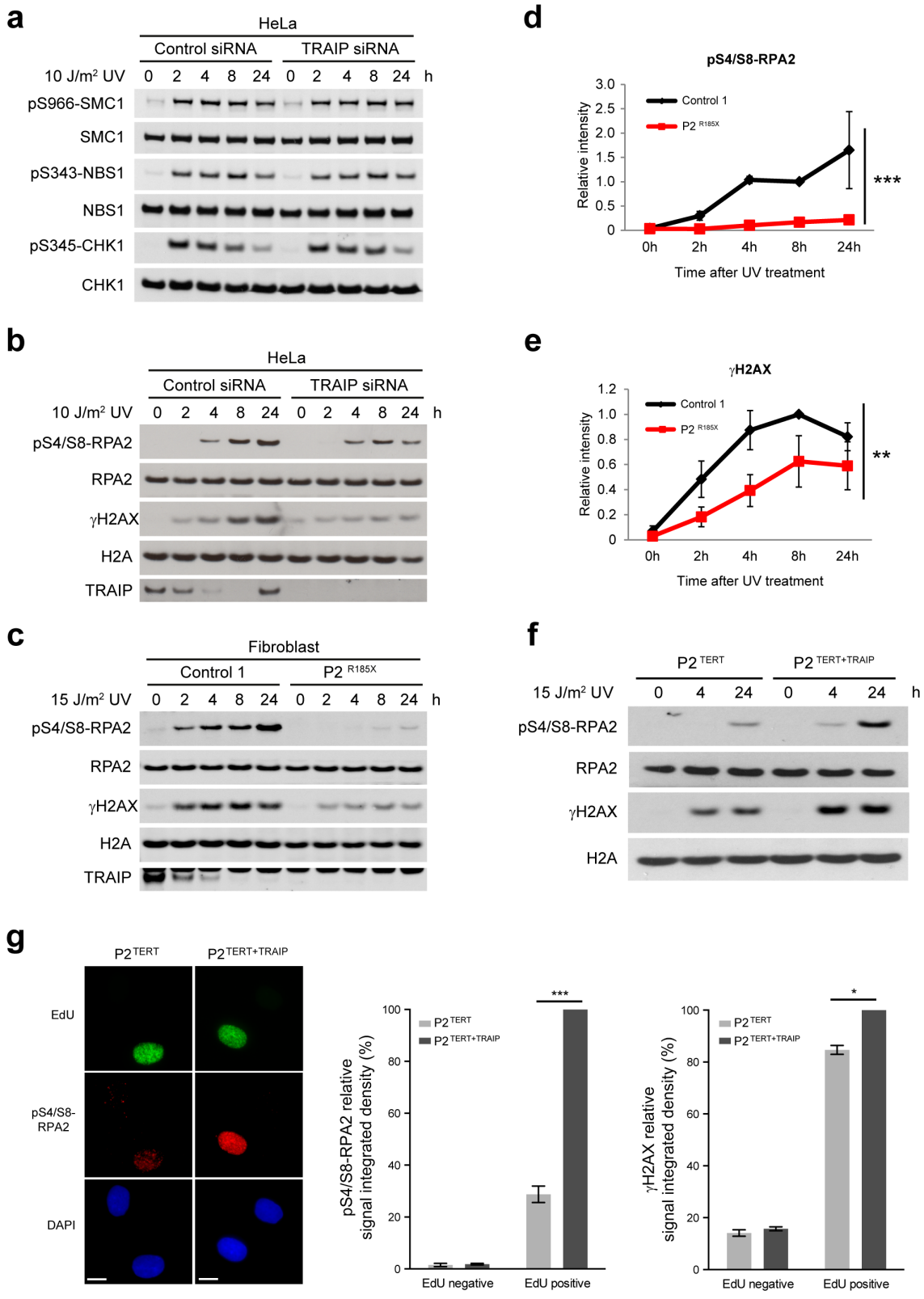
a
HeLa
Control siRNA
TRAIP siRNA
10 J/m² UV
0 2 4 8 24 0 2 4 8 24 h
pS966-SMC1
SMC1
pS343-NBS1
NBS1
pS345-CHK1
CHK1
b
HeLa
Control siRNA
TRAIP siRNA
10 J/m² UV
0 2 4 8 24 0 2 4 8 24 h
pS4/S8-RPA2
RPA2
γH2AX
H2A
TRAIP
c
Fibroblast
Control 1
P2 R185X
15 J/m² UV
0 2 4 8 24 0 2 4 8 24 h
pS4/S8-RPA2
RPA2
γH2AX
H2A
TRAIP
d
pS4/S8-RPA2
Control 1
P2 R185X
Relative intensity
3.0
2.5
2.0
1.5
1.0
0.5
0
***
0h 2h 4h 8h 24h
Time after UV treatment
e
γH2AX
Control 1
P2 R185X
Relative intensity
1.2
1.0
0.8
0.6
0.4
0.2
0
**
0h 2h 4h 8h 24h
Time after UV treatment
f
P2 TERT
P2 TERT+TRAIP
15 J/m² UV
0 4 24 0 4 24 h
pS4/S8-RPA2
RPA2
γH2AX
H2A
g
P2TERT
P2TERT+TRAIP
EdU
pS4/S8-RPA2
DAPI
pS4/S8-RPA2 relative signal integrated density (%)
100
80
60
40
20
0
P2TERT
P2TERT+TRAIP
***
EdU negative
EdU positive
γH2AX relative signal integrated density (%)
100
80
60
40
20
0
P2TERT
P2TERT+TRAIP
*
EdU negative
EdU positive

Figure 5

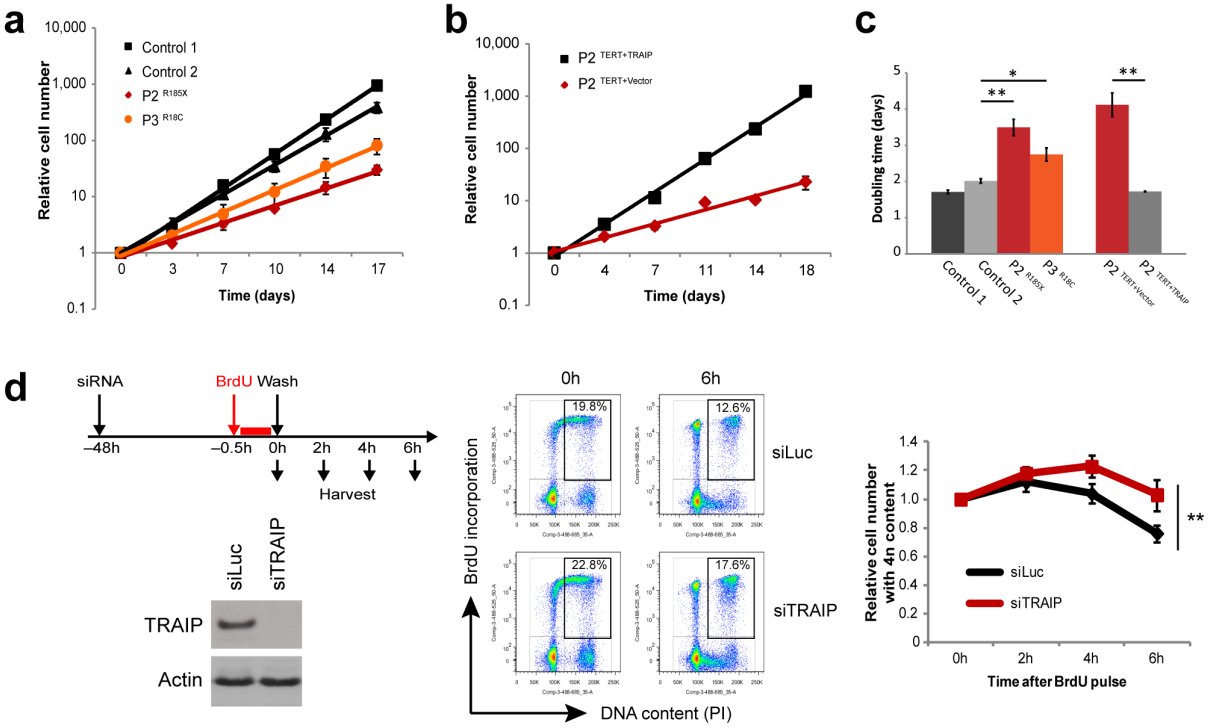
a
Relative cell number
Time (days)
Control 1
Control 2
P2 R185X
P3 R18C
b
Relative cell number
Time (days)
P2 TERT+TRAIP
P2 TERT+Vector
c
Doubling time (days)
Control 1
Control 2
P2 R185X
P3 R18C
P2 TERT+Vector
P2 TERT+TRAIP
d
siRNA
BrdU
Wash
–48h
–0.5h
0h
2h
4h
6h
Harvest
siLuc
siTRAIP
TRAIP
Actin
0h
6h
19.8%
12.6%
22.8%
17.6%
siLuc
siTRAIP
BrdU incorporation
DNA content (PI)
Relative cell number with 4n content
Time after BrdU pulse
siLuc
siTRAIP

Figure 6

a

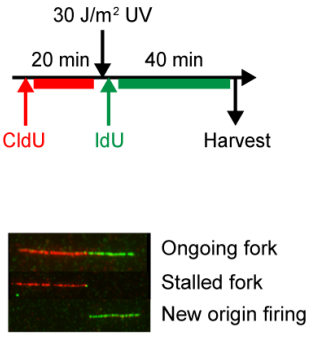
30 J/m² UV
20 min
40 min
CldU
IdU
Harvest
Ongoing fork
Stalled fork
New origin firing

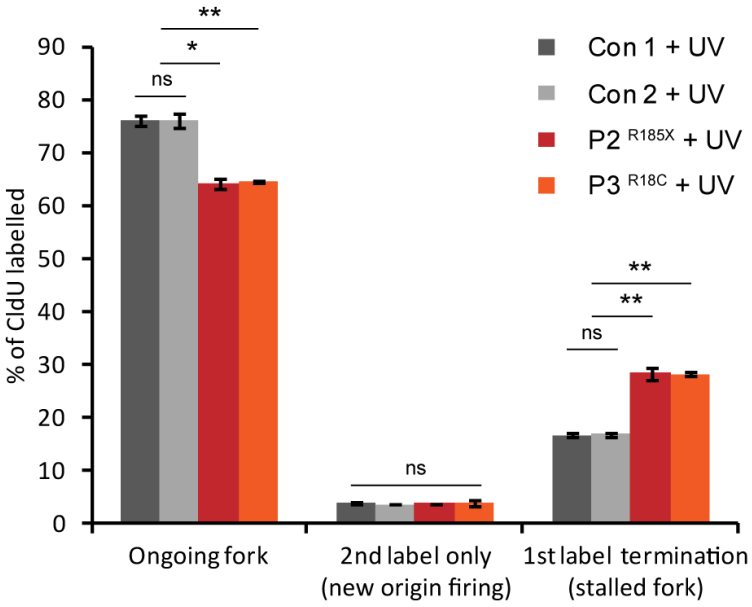
Con 1 + UV
Con 2 + UV
P2 R185X + UV
P3 R18C + UV
% of CldU labelled
0
10
20
30
40
50
60
70
80
90
**
*
ns
ns
**
**
ns
Ongoing fork
2nd label only
(new origin firing)
1st label termination
(stalled fork)

b

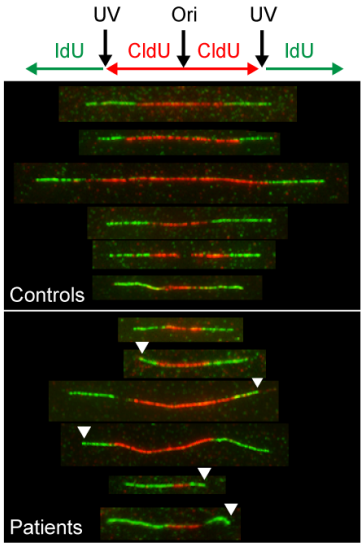
UV
Ori
UV
IdU
CldU
CldU
IdU
Controls
Patients

c

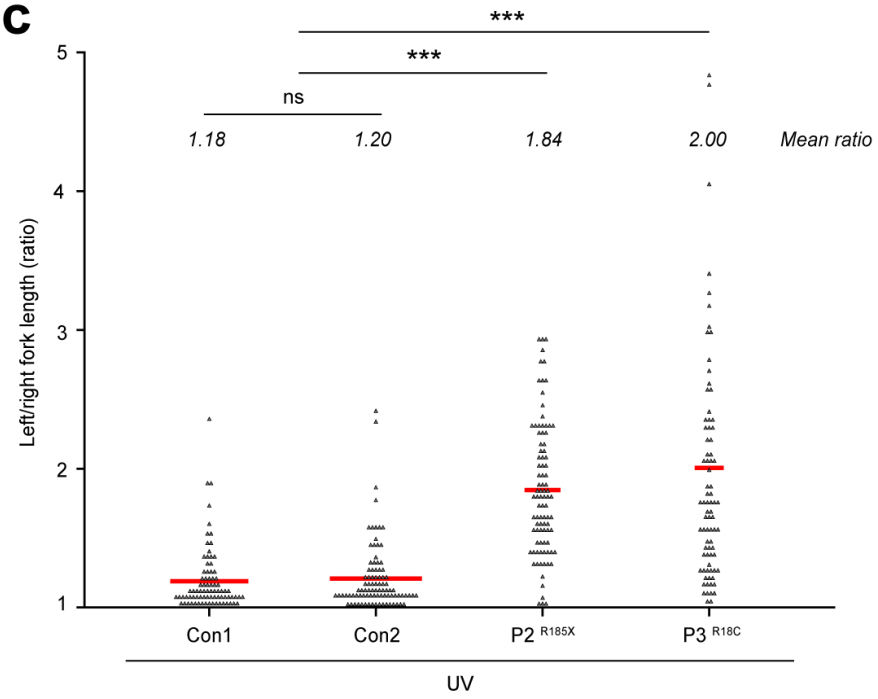
***
***
ns
1.18
1.20
1.84
2.00
Mean ratio
Left/right fork length (ratio)
1
2
3
4
5
Con1
Con2
P2 R185X
P3 R18C
UV

a

Probe ID	SNP	Mb	P1	P2
S-4FGGW	rs9862388	46.50	AB	AB
S-3TSZO		46.53	BB	BB
S-4FXOL	rs867619	46.54	AB	AA
S-4RJWK	rs10514713	46.54	AA	AA
[85 markers]				
S-4IYYA	rs2109181	48.58	AB	AA
S-3GGRR	rs9866124	48.60	AA	AA
S-3VSDU	rs7631574	48.66	BB	BB
S-4EVCN	rs28452701	48.71	AA	AA
S-3HTCL	rs4858831	48.74	BB	BB
S-4AVOY	rs6791542	48.79	BB	BB
S-3YZPW	rs58914641	48.94	BB	BB
[15 markers]				
S-3NGEJ	rs2271960	49.88	BB	BB
TRAIP		**49.88**	**XX**	**XX**
S-3MNNH	rs4688689	50.04	BB	BB
[87 markers]				
S-3ZJVS	rs12635140	52.74	AA	AA
S-4PFTZ	rs2019065	52.81	AA	AA
S-3CZNO	rs1042779	52.82	BB	BB
S-3GUUF	rs3733047	52.87	AA	AA
S-3JQFE	rs2336156	52.87	BB	-
S-4EQPB	rs60961047	52.89	BB	BB
S-3WAJS	rs35651539	52.93	BB	AA
[15 markers]				
S-3GIPO	rs7616077	53.18	AA	AA
S-3ZTFT	rs13084863	53.22	AB	BB
[139 markers]				
S-3DIBQ	rs4955903	54.91	AB	AA
S-4INOW	rs17054524	54.93	BB	BB
S-3QNFD	rs1969481	54.93	AB	AB

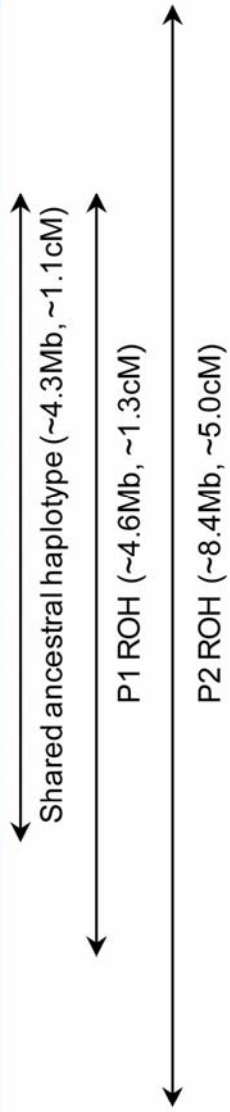

b

		P1	P2
F (FEstim)	**Average**	0	0.003
	Standard Error	-	0.002
F_{ROH}	**Average**	0.00098	0.00218
Inbreeding coefficient equivalent to		-	~3rd cousin

Supplementary Figure 1

Patients P1 and P2 have distant common ancestry, sharing a common 4.3 Mb homozygous haplotype across the TRAIP locus

(**a**) Schematic of high density SNP genotyping of the *TRAIP* locus in P1 and P2 (blue shading) demonstrates that both patients have 4.6 Mb and 8.4 Mb regions of homozygosity surround the TRAIP gene which lies at 49.9 Mb. An identical haplotype of 117 SNPs is

evident in both patients within the shared region of homozygosity consistent with a shared common ancestor. Heterozygous SNP markers delineating regions of homozygosity are shown in red. 102 homozygous SNP markers within the 4.3 Mb region are omitted for clarity. (**b**) Inbreeding coefficients (F) estimates for P1 and P2 from SNP genotype data. FEstim analysis software that utilizes hidden Markov chain maximum likelihood estimation approach on the basis of observed genome-wide marker genotypes[S3] was used to derive inbreeding coefficients for patient P1 and P2 from genome wide SNP genotyping data. An inbreeding coefficient of 0.003 was found for P2 that corresponds to an inbreeding coefficient seen in offspring of 3rd cousin parents. This estimate was confirmed by a complimentary approach that derives a statistic F_{ROH} from the percentage of the genome containing large regions of homozygosity, a measure that correlates well with inbreeding coefficients derived from pedigrees[S4]. Additionally, two point linkage analysis using the known family pedigree in P3 and a pedigree equating to the calculated inbreeding coefficient of 0.003 for P2, generates a significant combined LOD score of 4.42 at $\theta=0$.

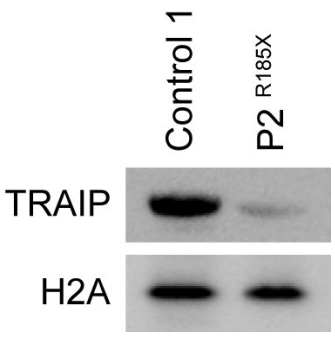

Supplementary Figure 2

TRAIP protein levels are markedly reduced in patient P2

Expression of TRAIP protein is only detectable on prolonged exposure of Western blots. Residual protein detected may include the isoform encoded by a transcript that skips exon 7. Deletion in this exon results in an in-frame deletion of 37 amino acids, which would be predicted to result in a 47 kDa protein that will be difficult to distinguish from the 53 kDa full-length TRAIP on immunoblotting. Immunoblotting performed on cell lysates using TRAIP and H2A (loading control) antibodies.

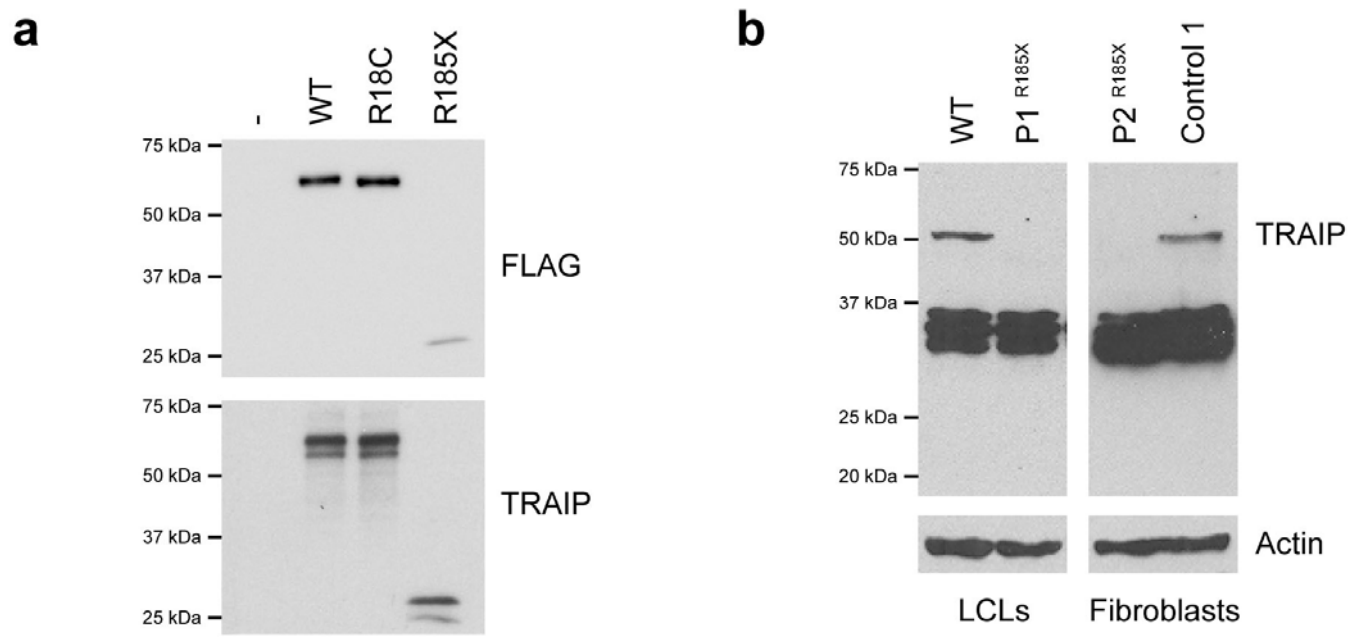

Supplementary Figure 3

A TRAIP polyclonal antibody raised against recombinant GST-TRAIP aa1-270, detects WT, Arg18Cys and Arg185*-truncated TRAIP proteins

(**a**) N-terminal FLAG-tagged TRAIP proteins, either WT or with patient mutations, were generated by *in vitro* transcription/translation (IVT) and then immunoblotted with either anti-FLAG or the rabbit polyclonal anti-TRAIP antibody generated in this study. Empty vector (-) was used as a negative control. The TRAIP antibody recognized all forms of TRAIP as efficiently as the anti-FLAG antibody, including the missense Arg18Cys mutation from patient P3 and the truncated TRAIP protein corresponding to aa1-184 that might be translated from transcripts containing the truncating Arg185* mutation in patients P1 and P2. WT and Arg18Cys were present at the same level (anti-FLAG) and detected equally well with TRAIP antibody, whereas Arg185* was present at a lower level (anti-FLAG), but still detected well with TRAIP antibody. The additional lower molecular band in each lane on the anti-TRAIP antibody blot likely results from untagged TRAIP protein generated during *in vitro* translation through usage of an alternative methionine start site, present immediately after the FLAG tag. (**b**) Full Western blots of patients P1 and P2 reveal no short truncated form of TRAIP protein, indicating that the mutated transcripts are most likely degraded via nonsense-mediated decay.

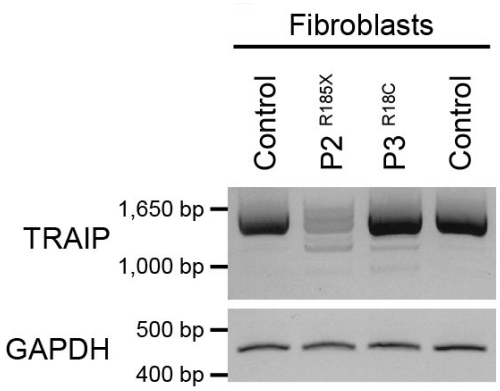

Supplementary Figure 4

TRAIP transcript levels in patient P3 primary fibroblasts are not depleted

RT-PCR using primers in 5' and 3' UTR to amplify *TRAIP* mRNA in primary fibroblasts demonstrates similar transcript levels in patient P3 cells when compared to control fibroblast cell line. Loading control, *GAPDH*.

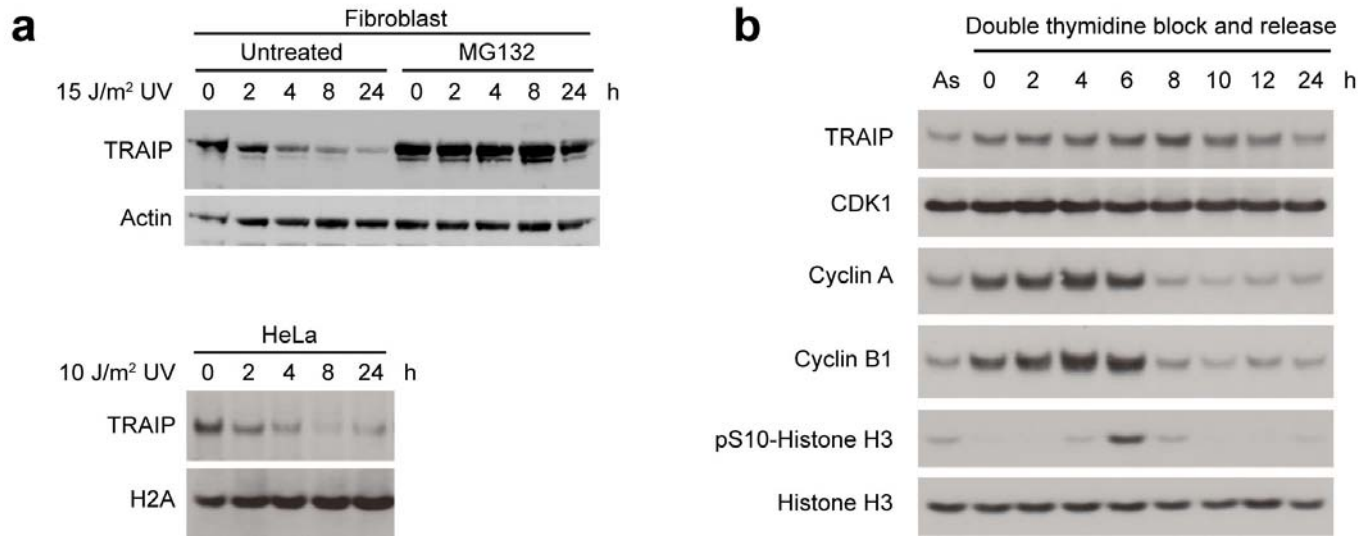

Supplementary Figure 5

TRAIP is degraded via the proteasome in response to UV damage

(**a**) Immunoblots of control fibroblast cells (upper panel) and HeLa cells (lower panel) treated with UV-C, before harvesting at the indicated times. The proteasome inhibitor MG132 (10 μM) was added to cell media at t=0 h. Cell lysates were analyzed by Western blot using antibodies against TRAIP and actin or H2A (loading controls). (**b**) Reduction in TRAIP protein levels is not accounted for by an indirect effect on cell cycle, as TRAIP protein levels remain relatively constant through the cell cycle. HeLa cells synchronized at the G1/S phase boundary by double thymidine block; time course following release into fresh media. Samples harvested at the indicated times and cell lysates analyzed by Western blot using antibodies against TRAIP, CDK1, cyclin A, cyclin B1, pSer10-Histone H3 and Histone H3.

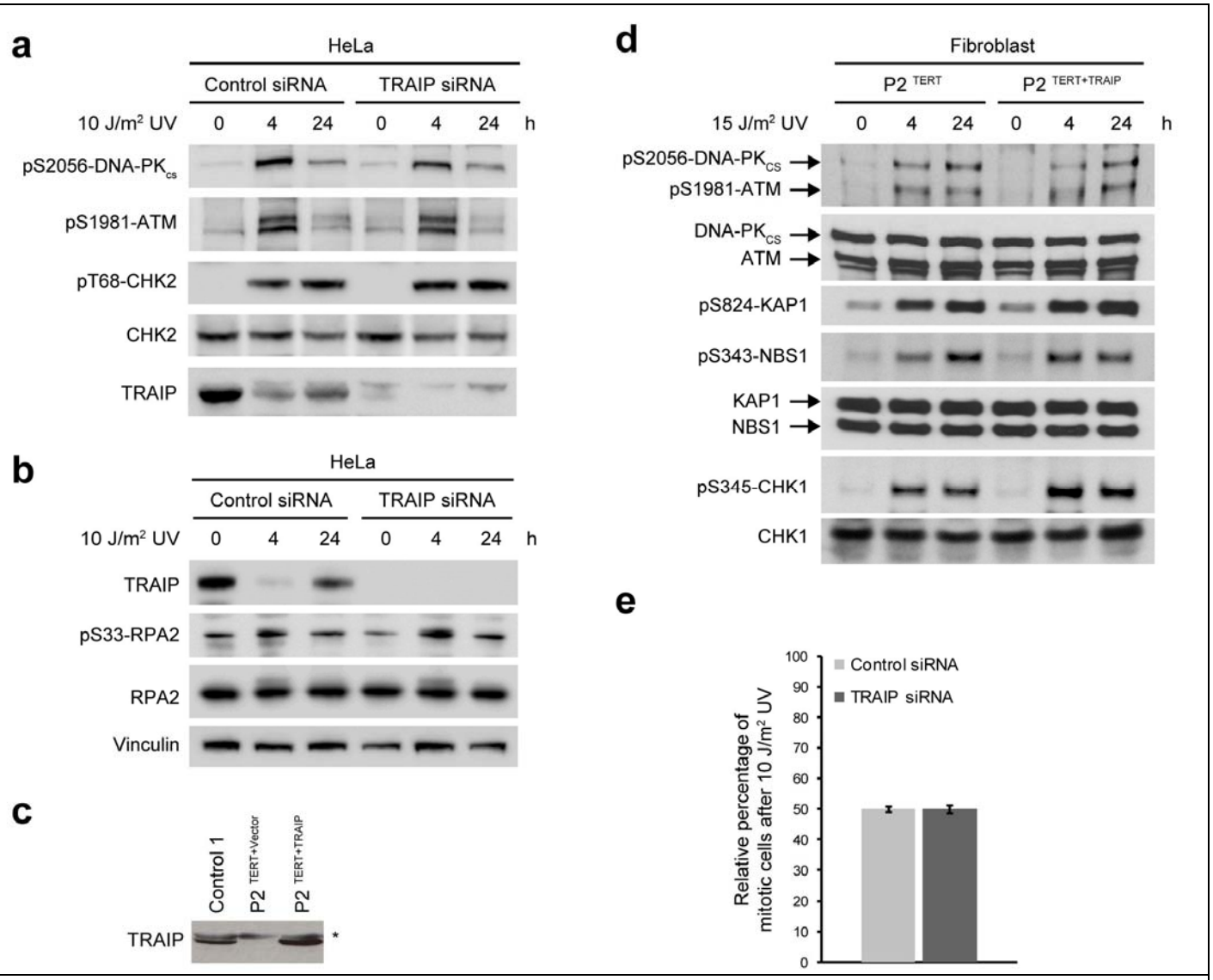

Supplementary Figure 6

TRAIP-deficient cells are generally proficient in ATM, DNA-PKcs and ATR signaling in response to UV-C

(**a**) TRAIP-depleted HeLa cells are proficient in ATM and DNA-PKcs signaling. HeLa cells were transfected with RNAi against TRAIP or luciferase (control). After 72h, cells were UV-C treated, before harvesting at indicated times. Cell lysates were analyzed by Western blot as indicated. (**b**) Phosphorylation of Ser33-RPA2 is unaffected by TRAIP depletion. HeLa cells transfected with RNAi against TRAIP or control were UV-C treated and harvested at indicated times. Cell lysates prepared using NP-40-based lysis buffer were analyzed by Western blot using antibodies against TRAIP, pSer33-RPA2, RPA2 and Vinculin. (**c**) TRAIP protein expression is restored in hTERT-immortalized patient fibroblasts following retroviral complementation with pMSCV-TRAIP. Western blots of patient fibroblasts after hTERT immortalization and retroviral transduction of pMSCV-vector only or pMSCV-TRAIP. * denotes a non-specific band. (**d**) Characterization of ATM, DNA-PKcs and ATR activation in $P2^{TERT}$ and $P2^{TERT+TRAIP}$ fibroblasts after UV-C irradiation. $P2^{TERT}$ and $P2^{TERT+TRAIP}$ fibroblasts were UV-C treated and harvested at indicated times. Cell lysates were analyzed by Western blot as indicated. ATM and DNA-PKcs autophosphorylation and NBS1 and KAP1 phosphorylation were similar in both cell lines, while a small reduction in CHK1 phosphorylation was observed in $P2^{TERT}$ cells. (**e**) TRAIP-depleted HeLa cells are proficient in G2/M checkpoint assay. Mitotic index is unchanged in TRAIP-depleted HeLa cells (plotted relative to the mitotic index of untreated cells in the same experiment). Mean ± SEM; n=3 independent experiments.

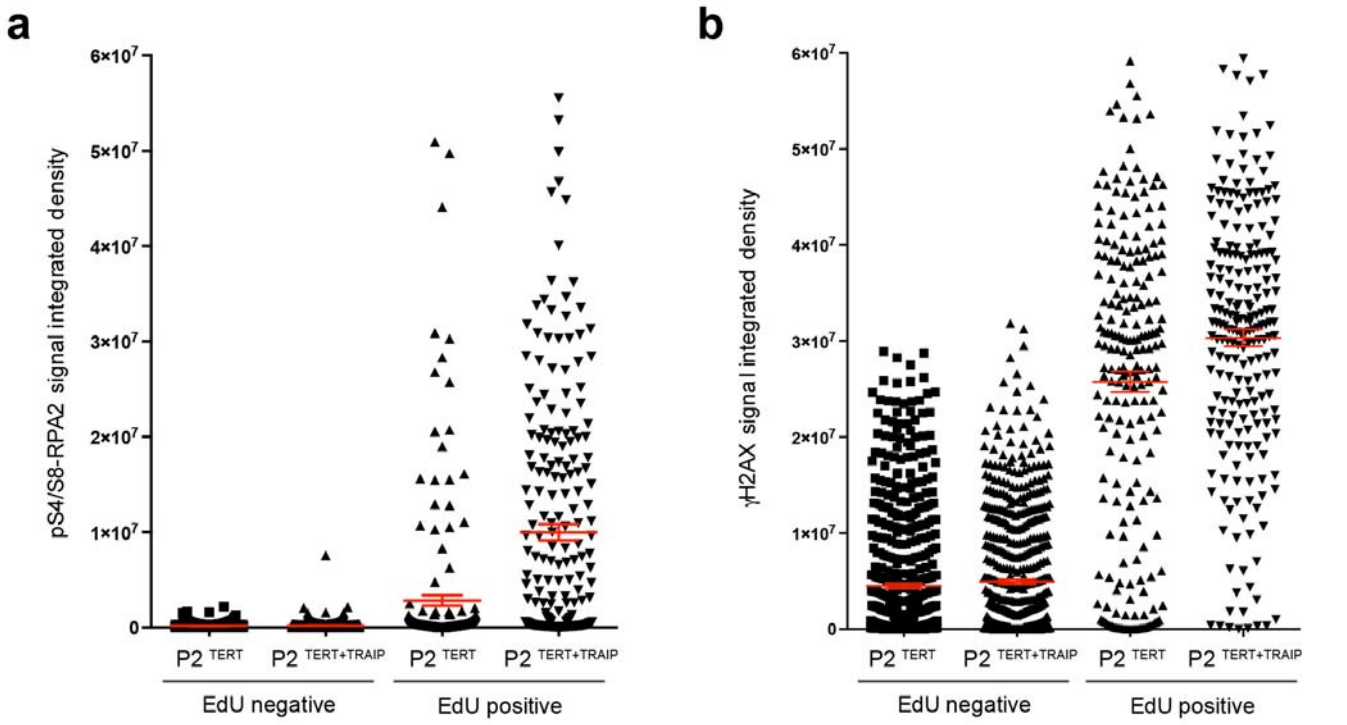

Supplementary Figure 7

TRAIP promotes S-phase specific RPA2 and H2AX phosphorylation induced by UV-C

(a, **b)** Scatter plots represent pSer4/Ser8-RPA2 (**a**) or γH2AX (**b**) signal integrated densities (arbitrary units) of individual EdU-negative and EdU-positive $P2^{TERT}$ and $P2^{TERT+TRAIP}$ fibroblasts shown in Figure 4g. Red lines denote mean ± SEM for n=3 independent experiments. Pooled data plotted, n>50 EdU positive cells and n>150 EdU negative cells quantified per cell line per treatment per experiment.

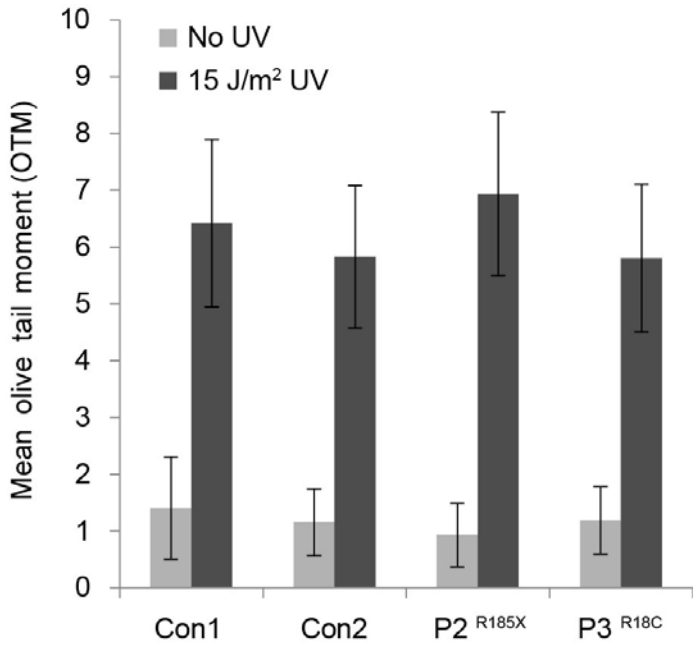

Supplementary Figure 8

TRAIP mutations do not detectably alter the accumulation of DNA strand breaks following UV-C treatment

Primary patient fibroblasts or controls were UV-C treated and harvested 4 h later for neutral comet assay. Graph represents quantification of mean olive tail moments ± SEM for n=4 independent experiments. >250 comets analyzed per cell line per treatment.

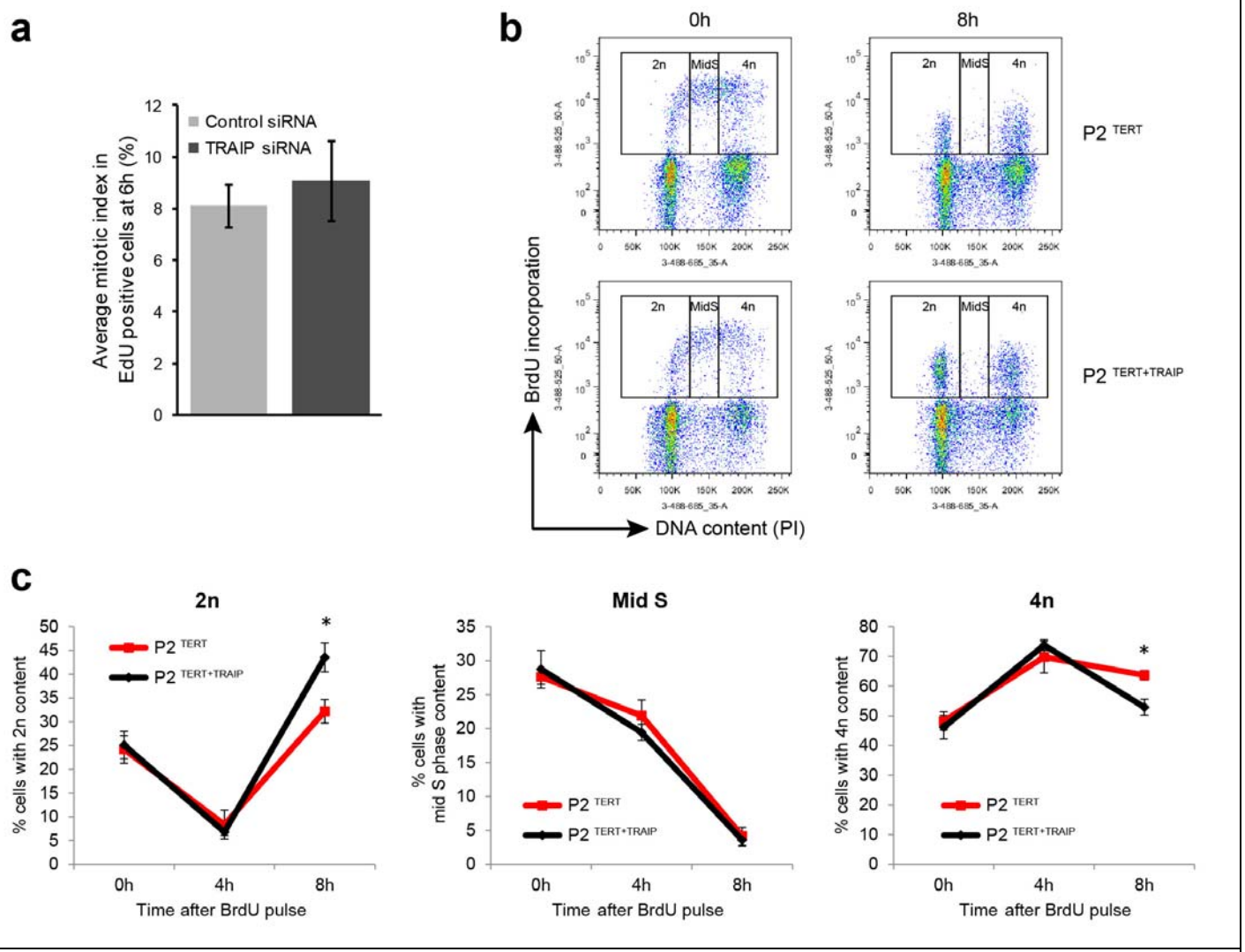

Supplementary Figure 9

TRAIP-deficiency delays cell cycle progression in S/G2

(**a**) Quantification of number of mitotic cells contributing to 4n cell number at 6 h in Figure 5d. The mitotic index of siTRAIP EdU positive cells 6 h after EdU pulse labeling is not significantly different from control siRNA treated cells. Mean ± SEM of n=3 independent experiments; >800 EdU positive cells quantified per experiment. (**b**, **c**) Complementation with TRAIP restores delayed S/G2 phase progression of $P2^{TERT}$ fibroblasts. $P2^{TERT}$ and $P2^{TERT+TRAIP}$ cells were labeled with 10 μM BrdU for 30 min before washing out and replacing with fresh media. At indicated times, cells were harvested, fixed and prepared for flow cytometry. (**b**) Representative images of gating used in analysis of flow cytometry data. (**c**) Quantification of BrdU positive cells at 0, 4 and 8 h after BrdU pulse labeling. Left, percentage of cells with 2n content; middle, percentage of cells with mid S phase content; right, percentage of cells with 4n content. Mean ± SEM of n=4 independent experiments; for 8 h time point, Student's *t*-test: *p<0.05.

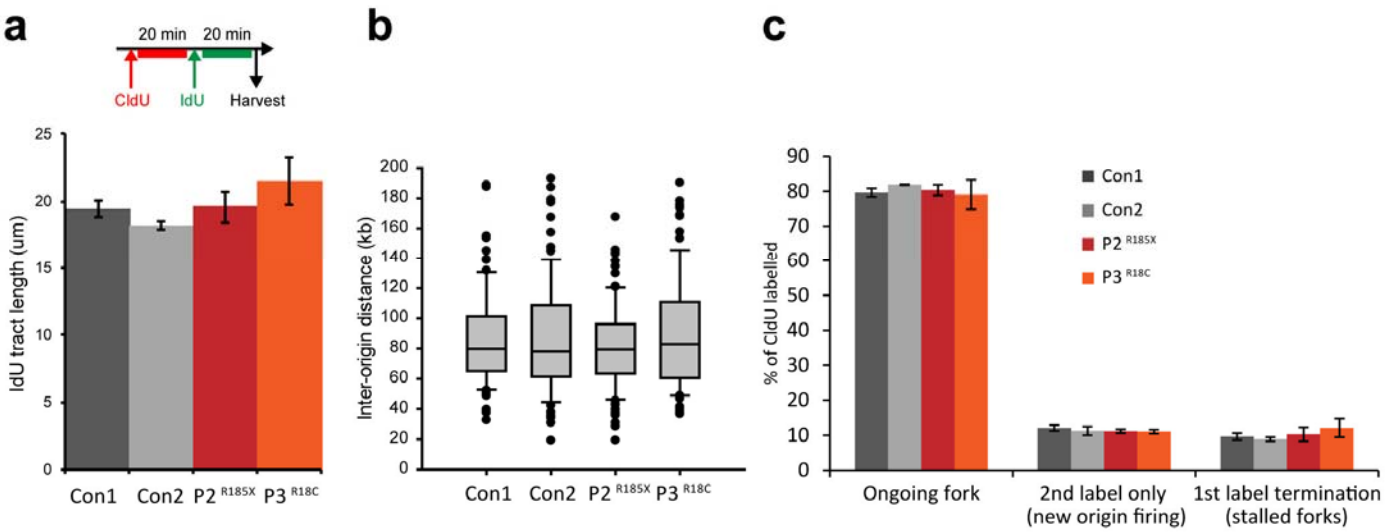

Supplementary Figure 10

Fork velocity, inter-origin distance and new origin synthesis rates are unaltered in TRAIP patient primary fibroblasts

(**a**) Top panel, schematic indicating DNA labeling protocol. Bottom panel, quantification of IdU tract lengths in control and patient fibroblasts. Mean ± SEM of n=3 independent experiments; >100 fibers measured per cell line per experiment. (**b**) Quantification of inter-origin distances. Box plots, center lines indicate mean, box 25/75% and whiskers 5/95%. n=3 independent experiments; >30 structures measured per cell line per experiment. (**c**) Quantification of ongoing forks, 2nd label only (new origin firing) and 1st label termination (fork stalling) structures. Mean ± SD, n=3 independent experiments; > 300 fibers measured per cell line per experiment.

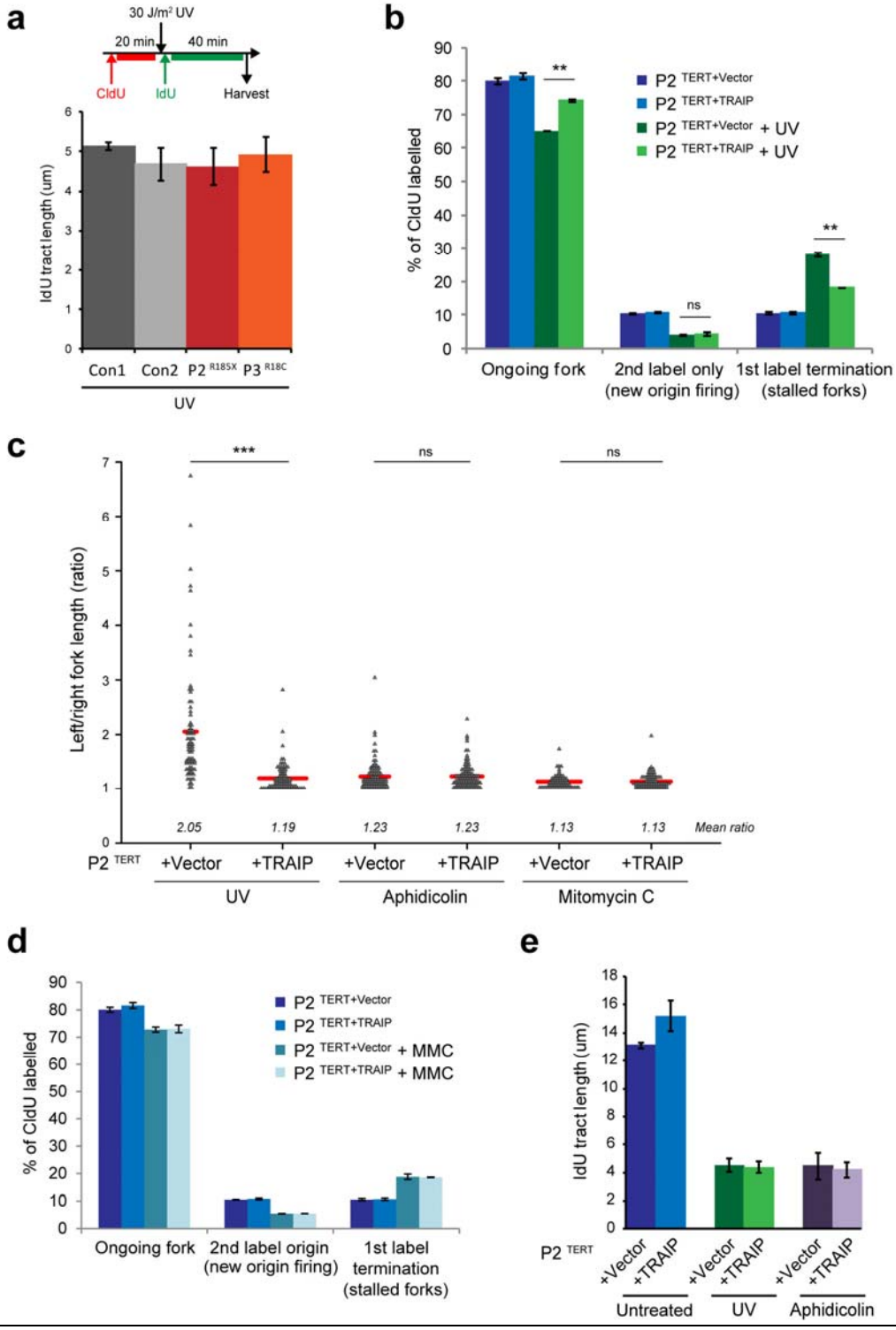

Supplementary Figure 11

Complementation with wild-type TRAIP rescues increased fork stalling and fork asymmetry in UV-irradiated TRAIP^{Arg185*} cells

(**a**) Fork velocities in UV-treated TRAIP patient primary fibroblasts are similar to wild-type control cells. Mean ± SEM, n=2 independent experiments, >100 structures measured per cell line per experiment. (**b**) Quantification of ongoing forks, 2nd label only (new origin

firing) and 1st label termination (fork stalling) structures, untreated or after 30 J/m^2 UV-C irradiation. Mean ± SD, n=3 independent experiments. >400 structures measured per cell line per experiment. Student's *t*-test: **p<0.01; ns, not significant. (**c**) Quantification of replication fork asymmetry in P2^{TERT} and P2$^{TERT+TRAIP}$ fibroblasts after 30 J/m^2 UV, 0.5 μM aphidicolin or 50 ng/ml mitomycin C treatment. Ratio of left/right fork length; mean ratio for each cell line is indicated in italics; Mann Whitney Rank sum test: ***p<0.001; ns, not significant. Data plotted pooled from n=2 independent experiments, with >50 structures quantitated per cell line per experiment. (**d**) Quantification of ongoing forks, 2nd label only (new origin firing) and 1st label termination (stalled fork) structures, untreated or after 50 ng/ml mitomycin C treatment. (**e**) Track lengths are not detectably altered in TRAIP-deficient fibroblasts compared with controls, after UV-C or low dose aphidicolin treatment. P2^{TERT} and P2$^{TERT+TRAIP}$ fibroblasts untreated or following treatment with 30 J/m^2 UV or 0.5 μM aphidicolin. Mean ± SEM, n=2 independent experiments. >100 tracts measured per cell line per experiment.

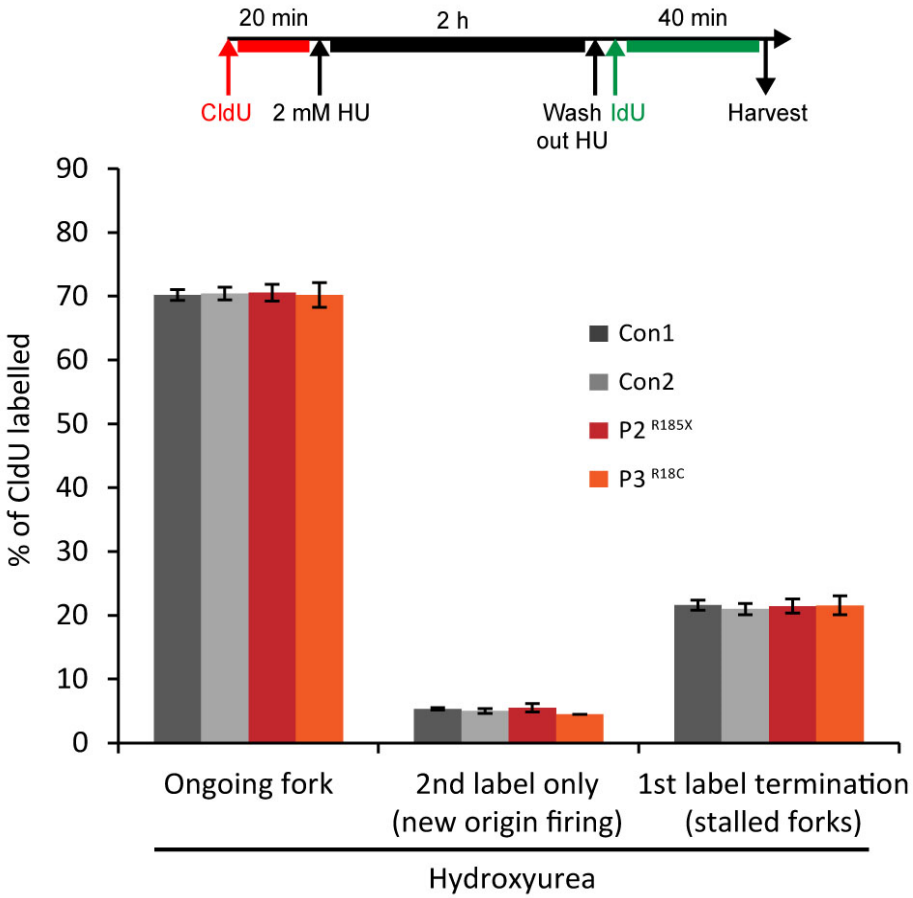

Supplementary Figure 12

Replication restart is not impaired in TRAIP patient cells after hydroxyurea-induced fork arrest

Top, schematic of the experiment. Bottom, quantification of ongoing forks, 2nd label only (new origin firing) and 1st label termination (fork stalling) structures. Data are mean ± SD for n=2 independent experiments. >300 structures quantified per cell line per experiment.

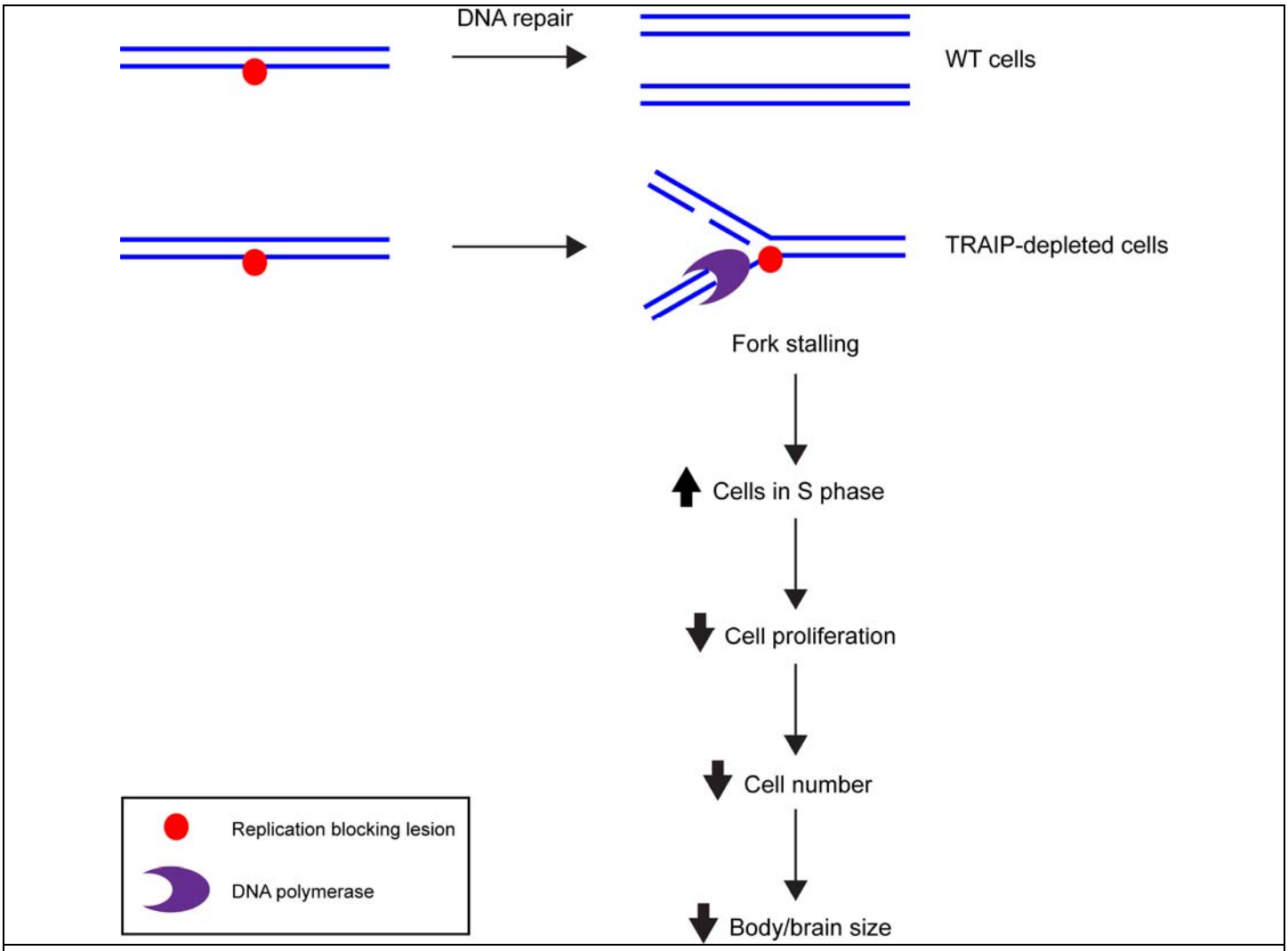

Supplementary Figure 13

Model: Impaired DNA damage response to replication blocking lesions such as UV photodimers in TRAIP patient cells can reduce growth through reduction in cell number generated during development

Replication blocking lesions (red circles) arise in the genome during development, which require efficient DDR for their resolution and to ensure efficient cellular proliferation utilizing multiple repair pathways that include translesion synthesis/post-replication repair. In TRAIP patient cells, impaired DDR during replication results in delayed S/G2 phase progression. Increased cell cycle length and reduced numbers of cycling cells will consequently lead to reduction in overall cell proliferation, decreasing total cell number. Impaired spindle checkpoint function could also increase aneuploidy levels leading to increased cell death[S5]. However, unlike mutations in BUBR1[S6], an archetypal SAC protein, variegate aneuploidy is not observed with normal karyotypes in all TRAIP patients (**Table 1**). Decrease in cell number results in diminished growth potential, with reduction in both brain and body size.

Supplementary Note. Summary of clinical phenotypes

All patients had IUGR (birth weight ranging from -2.2 to -2.9 SD) and postnatally substantially reduced height (range -3.9 to -5.4 SD) with disproportionate microcephaly (range -6.5 to -8.3 SD). Growth parameters were therefore consistent with microcephalic primordial dwarfism, particularly with that seen within the primary microcephaly-Seckel syndrome spectrum[S1]. In addition, P1 had two siblings with IUGR, microcephaly and facial features consistent with Seckel syndrome, both of whom died in early infancy as a result of respiratory failure. The clinical features of these siblings have been previously reported[S2]; however DNA was not available to confirm the presence of TRAIP mutations in these two siblings.

All three individuals had similar phenotypic features with long narrow faces, micrognathia and prominent ears. P1 and P2 additionally had scaphocephaly. Mild-moderate developmental delay was present in all. In P2 and P3, neuroimaging demonstrated reduced cerebral cortical size, without thickening of the cortex, consistent with 'microcephaly with simplified gyri' in P2 and P3. In P1, a small cyst between the anterior and posterior pituitary and a slightly enlarged ventricular system were noted.

P1 and P2 experienced frequent lower respiratory tract infections. These required multiple intensive care admissions for P2, with respiratory syncytial infection specifically identified in one such admission. P1 and P2 both had chronic chest X-ray changes; chest CT showing atelectasis with mediastinal shift in P1. Medical management of P2 included prophylactic antibiotics. Respiratory care of P1 included regular chest physiotherapy, inhaled corticosteroid treatment and prophylactic antibiotics. This patient passed away secondary to acute respiratory failure aged 8 years. A diagnosis of asthma has been made for P3 who also has a history of recurrent urinary tract infections. Aside from a mild lymphopenia, not thought to be of clinical significance in P2, no evidence of immunodeficiency was detected in any of the patients. All patients had normal immunoglobulin levels.

Karyotypes from P1-P3 were reported as normal. A trial of GH in P1 did not lead to increased growth velocity.

Supplementary Table 1. Primer sequences related to experimental procedures

a) siRNA oligonucleotide sequences		
Name		
siTRAIP-524	AGCAGAUGAAGUACUUAGA[dT][dT]	
siLuciferase	CUUACGCUGAGUACUUCGA[dT][dT]	
b) RT-PCR primer sequences		
Name	**Forward sequence**	**Reverse sequence**
TRAIP-5'UTR and -3'UTR	CCTTGAGTCCAGCCATCATGCCTATCC	GGCCATTGGTCAGACTCACTGTTC
GAPDH	GGACTCCACGACGTACTCAGCGCCAGC	GTGGATATTGTTGCCATCAATGACC

Supplementary References

S1. Verloes, A., Drunat, S., Gressens, P. & Passemard, S. Primary Autosomal Recessive Microcephalies and Seckel Syndrome Spectrum Disorders. in *GeneReviews(R)* (eds. Pagon, R.A. *et al.*) (Seattle (WA), 1993).

S2. Silengo, M., Del Monaco, A., Linari, A. & Lala, R. Low birth-weight, microcephalic malformation syndrome in a 46,XX girl and her 46,XY sister with agonadism: third report of the Kennerknecht syndrome or autosomal recessive Seckel-like syndrome with previously undescribed genital anomalies. *Am J Med Genet* **101**, 275-278 (2001).

S3. Leutenegger, A.L. *et al.* Using genomic inbreeding coefficient estimates for homozygosity mapping of rare recessive traits: application to Taybi-Linder syndrome. *Am J Hum Genet* **79**, 62-66 (2006).

S4. McQuillan, R. *et al.* Runs of homozygosity in European populations. *Am J Hum Genet* **83**, 359-372 (2008).

S5. Chapard, C. *et al.* The TRAF-interacting protein (TRAIP) is a regulator of the spindle assembly checkpoint. *J Cell Sci* **127**, 5149-5156 (2014).

S6. Hanks, S. *et al.* Constitutional aneuploidy and cancer predisposition caused by biallelic mutations in BUB1B. *Nat Genet* **36**, 1159-1161 (2004).